OXFORD GENETICS

GENETICS, 2021, 217(1), iyaa028
DOI: 10.1093/genetics/iyaa028
Advance Access Publication Date: 22 December 2020
Investigation

Regulation of growth and cell fate during tissue regeneration by the two SWI/SNF chromatin-remodeling complexes of *Drosophila*

Yuan Tian[1] and Rachel K. Smith-Bolton[1,2,*]

[1]Department of Cell and Developmental Biology, University of Illinois at Urbana-Champaign, Urbana, IL 61801, USA
[2]Carl R. Woese Institute for Genomic Biology, University of Illinois at Urbana-Champaign, Urbana, IL 61801, USA

*Corresponding author: Department of Cell and Developmental Biology, University of Illinois at Urbana-Champaign, 601 S. Goodwin Avenue, Urbana, IL 61801, USA. rsbolton@illinois.edu

Abstract

To regenerate, damaged tissue must heal the wound, regrow to the proper size, replace the correct cell types, and return to the normal gene-expression program. However, the mechanisms that temporally and spatially control the activation or repression of important genes during regeneration are not fully understood. To determine the role that chromatin modifiers play in regulating gene expression after tissue damage, we induced ablation in *Drosophila melanogaster* imaginal wing discs, and screened for chromatin regulators that are required for epithelial tissue regeneration. Here, we show that many of these genes are indeed important for promoting or constraining regeneration. Specifically, the two SWI/SNF chromatin-remodeling complexes play distinct roles in regulating different aspects of regeneration. The PBAP complex regulates regenerative growth and developmental timing, and is required for the expression of JNK signaling targets and the growth promoter *Myc*. By contrast, the BAP complex ensures correct patterning and cell fate by stabilizing the expression of the posterior gene *engrailed*. Thus, both SWI/SNF complexes are essential for proper gene expression during tissue regeneration, but they play distinct roles in regulating growth and cell fate.

Keywords: regeneration; chromatin; SWI/SNF complexes; Drosophila; wing imaginal disc

Introduction

Regeneration is a complex yet highly elegant process that some organisms can use to recognize, repair, and replace missing or damaged tissue. Imaginal disc repair in *Drosophila* is a good model system for understanding regeneration due to the high capacity of these tissues to regrow and restore complex patterning, as well as the genetic tools available in this model organism (Hariharan and Serras 2017). Regeneration requires the coordinated expression of genes that regulate the sensing of tissue damage, induction of regenerative growth, repatterning of the tissue, and coordination of regeneration with developmental timing. Initiation of regeneration in imaginal discs requires known signaling pathways such as the Reactive oxygen species (ROS), Jun N-terminal kinase (JNK), Wingless (Wg), p38, Janus kinase/signal transducer and activator of transcription (Jak/STAT), and Hippo pathways (Bosch *et al.* 2008; Smith-Bolton *et al.* 2009; Bergantinos *et al.* 2010; Schubiger *et al.* 2010; Grusche *et al.* 2011; Sun and Irvine 2011; Katsuyama *et al.* 2015; Santabárbara-Ruiz *et al.* 2015). These pathways activate many regeneration genes, such as the growth promoter *Myc* (Smith-Bolton *et al.* 2009) and the hormone-like peptide *ilp8*, which delays pupariation after imaginal disc damage (Colombani *et al.* 2012; Garelli *et al.* 2012). However, misregulation of these signals can impair regeneration. For example, elevated levels of JNK signaling can induce patterning defects in the posterior of the wing (Schuster and Smith-Bolton 2015), and elevated ROS levels can suppress JNK activity and regenerative growth (Brock *et al.* 2017). While the signals that initiate regeneration have been extensively studied, regulation of regeneration gene expression in response to tissue damage is not fully understood.

Such regulation could occur through chromatin modification. In *Drosophila*, chromatin modifiers include the Polycomb repressive complexes PRC1 and PRC2, which can be recruited to specific locations by the Pho repressor complex (PhoRC), the activating complexes Trithorax acetylation complex (TAC1), Complex of proteins associated with Set1 (COMPASS) and COMPASS-like, the nucleosome remodeling complex (NURF), and the switch/sucrose non-fermentable (SWI/SNF) chromatin remodelers Brahma-associated proteins (BAP) and Polybromo-associated proteins (PBAP) (Xiao *et al.* 2001; Kassis *et al.* 2017). PRC2 carries out trimethylation of histone H3 at lysine 27, recruiting PRC1 to repress transcription of nearby genes. COMPASS-like and COMPASS carry out histone H3 lysine 4 monomethylation and di- and trimethylation, respectively, thereby activating the expression of nearby genes. TAC1 acetylates histone H3 lysine 27, also supporting activation of gene transcription. NURF, BAP, and PBAP alter or move

Received: April 29, 2020. **Accepted:** November 10, 2020

nucleosomes to facilitate binding of transcription factors and chromatin modifiers (Xiao *et al.* 2001; Kassis *et al.* 2017). Rapid changes in gene expression induced by these complexes may help facilitate a damaged tissue's regenerative response.

A few chromatin modifiers and histone modifications have been reported to be important for regulating regeneration of *Xenopus* tadpole tails, mouse pancreas and liver, zebrafish fins, and *Drosophila* imaginal discs (Wang *et al.* 2008; Stewart *et al.* 2009; Blanco *et al.* 2010; Scimone *et al.* 2010; Tseng *et al.* 2011; Fukuda *et al.* 2012; Pfefferli *et al.* 2014; Jin *et al.* 2015; Skinner *et al.* 2015). Furthermore, components of *Drosophila* and mouse SWI/SNF complexes regulate regeneration in the *Drosophila* midgut and mouse skin, liver, and ear (Jin *et al.* 2013; Xiong *et al.* 2013; Sun *et al.* 2016). However, little is known about how these complexes alter gene expression, signaling, and cellular behavior to regulate regeneration. Importantly, genome-wide analysis of chromatin state after *Drosophila* imaginal disc damage revealed changes in chromatin around a large set of genes, including known regeneration genes (Vizcaya-Molina *et al.* 2018). Thus, chromatin modifiers likely play a key role in regulating activation of the regeneration program. However, it is unclear whether all regeneration genes are coordinately regulated in the same manner, or whether specific chromatin modification complexes target different subsets of genes that respond to tissue damage.

To probe the role of chromatin modifiers in tissue regeneration systematically, we assembled a collection of pre-existing *Drosophila* mutants and RNAi lines targeting components of these complexes as well as other genes that regulate chromatin, and screened these lines for regeneration defects using the *Drosophila* wing imaginal disc. We used a spatially and temporally controllable tissue-ablation method that uses transgenic tools to induce tissue damage only in the wing primordium (Smith-Bolton *et al.* 2009). This method ablates 94% of the wing primordium on average at the early third instar and allows the damaged wing discs to regenerate *in situ*. Previous genetic screens using this tissue ablation method have identified genes critical for regulating different aspects of regeneration, such as *taranis*, *trithorax*, and *cap-n-collar*, demonstrating its efficacy in finding regeneration genes (Schuster and Smith-Bolton 2015; Skinner *et al.* 2015; Brock *et al.* 2017).

Through this targeted genetic screen of chromatin regulators, we found that mutations in *Drosophila* SWI/SNF components caused striking regeneration defects. The SWI/SNF complexes are conserved multi-subunit protein complexes that activate or repress gene expression (Wilson and Roberts 2011) by using the energy from ATP hydrolysis to disrupt histone-DNA contacts and remodel nucleosome structure and position (Côté *et al.* 1994; Kwon *et al.* 1994). Brahma (Brm) is the only ATPase of the SWI/SNF complexes in *Drosophila* (Tamkun *et al.* 1992; Kassis *et al.* 2017). Moira (Mor) serves as the core scaffold of the complexes (Mashtalir *et al.* 2018). Other components contain domains involved in protein–protein interactions, protein–DNA interactions, or interactions with modified histones (Hargreaves and Crabtree 2011). There are two subtypes of SWI/SNF in *Drosophila*: the Brahma-associated proteins (BAP) and the Polybromo-associated BAP (PBAP) remodeling complexes (Collins and Treisman 2000; Mohrmann *et al.* 2004). They share common core components, including Brm, Snf5-related 1 (Snr1), Mor, Brahma-associated protein 55kD (Bap55), Brahma-associated protein 60kD (Bap60), Brahma-associated protein 111kD (Bap111), and Actin (Mohrmann *et al.* 2004), but contain different signature proteins. The PBAP complex is defined by the components Brahma-associated protein 170kD (Bap170), Polybromo, and Supporter of activation of yellow protein (Sayp) (Mohrmann *et al.* 2004; Chalkley *et al.* 2008). Osa defines the BAP complex (Collins *et al.* 1999; Vázquez *et al.* 1999).

Here, we show that the SWI/SNF complexes BAP and PBAP are required for regeneration, and that the two complexes play distinct roles. The PBAP complex is important for activation of JNK signaling targets such as *ilp8* to delay metamorphosis and allow enough time for the damaged tissue to regrow, and for expression of *Myc* to drive regenerative growth. By contrast, the BAP complex functions to prevent changes in cell fate induced by tissue damage through stabilizing expression of the posterior identity gene *engrailed*. Thus, different aspects of the regeneration program are regulated independently by distinct chromatin regulators.

Materials and methods

Fly stocks

The following fly stocks were obtained for this study. In some cases, they were rebalanced before performing experiments: w^{1118};; *rnGAL4, UAS-rpr, tubGAL80^{ts}/TM6B, tubGAL80* (Smith-Bolton *et al.* 2009), w^{1118} (Wild type), *w*; P{neoFRT}82B osa^{308}/TM6B, Tb^{1}* (Bloomington *Drosophila* stock center, BL#5949) (Treisman *et al.* 1997), *w*; Bap170$^{\Delta 135}$/T(2; 3)SM6a-TM6B, Tb^{1}* was a gift from Jessica E. Treisman (Carrera *et al.* 2008), *brm^{2} e^{s} ca^{1}/TM6B, Sb^{1} Tb^{1} ca^{1}* (BL#3619) (Kennison and Tamkun 1988), *mor^{1}/TM6B, Tb^{1}* (BL#3615) (Kennison and Tamkun 1988), *y^{1} w^{1}; P{neoFRT}40A P{FRT(w^{hs})}G13 cn^{1} PBac{SAstopDsRed}Bap55^{LL05955} bw^{1}/CyO, bw^{1}* (BL#34495) (Schuldiner *et al.* 2008), *bap111* RNAi (Vienna *Drosophila* Resource Center, VDRC#104361), control RNAi background (VDRC#15293), *bap60* RNAi (VDRC#12673), *brm* RNAi (VDRC#37721), *P{PZ}tara^{03881} ry^{506}/TM3, ry^{RK} Sb^{1} Ser^{1}* (BL#11613) (Gutierrez 2003), *UAS-tara* was a gift from Michael Cleary (Manansala *et al.* 2013), *TRE-Red* was a gift from Dirk Bohmann (Chatterjee and Bohmann 2012). *mor^{2}*, *mor^{11}* and *mor^{12}* alleles were gifts from James Kennison (Kennison and Tamkun 1988), *snr1^{E2}* and *snr1^{SR21}* alleles were gifts from Andrew Dingwall (Zraly *et al.* 2003). *Df(3R)RD31/Dp(3; 3)S462, In(3LR)EBL, In(3R)C, Sb^{1} ca^{1}* (Hopmann *et al.* 1995) (BL#5127), *w^{1118}; Df(3R)BSC790, P+PBac{w[+mC]=XP3.WH3}BSC790/TM6C, Sb^{1} cu^{1}* (Cook *et al.* 2012) (BL#27362), *ry^{506} P {PZ}osa^{00090}/TM3, ry^{RK} Sb^{1} Ser^{1}* (Spradling *et al.* 1995) (BL#11486).

The mutants and RNA interference lines in Supplementary Table S1 used for the chromatin regulator screen were:

st^{1} in^{1} kni^{ri-1} Scr^{W} Pc^{3}/TM3, Sb^{1} Ser^{1} (BL#3399),
cn^{1} Psc^{1} bw^{1} sp^{1}/CyO (BL#4200),
y^{1} w; P{neoFRT}42D Psc^{e24}/SM6b, P{eve-lacZ8.0}SB1* (BL#24155),
w; P{neoFRT}82B Abd-B^{Mcp-1} Sce^{1}/TM6C, Sb^{1} Tb^{1}* (BL#24618),
w; P{neoFRT}82B Scm^{D1}/TM6C, Sb^{1} Tb^{1}* (BL#24158),
w; E(z)^{731} P{1xFRT.G}2A/TM6C, Sb^{1} Tb^{1}* (BL#24470),
w; Su(z)12^{2} P{FRT(w^{hs})}2A/TM6C, Sb^{1} Tb^{1}* (BL#24159),
esc^{21} b^{1} cn^{1}/In(2LR)Gla, wg^{Gla-1}; ca^{1} awd^{K} (BL#3623),
y^{1} w^{67c23}; P{wHy}Caf1-55^{DG25308} (BL#21275),
w^{1118}; P{XP}escl^{d01514} (BL#19163),
y^{1} w; phol^{81A}/TM3, Ser^{1} y^{+}* (BL#24164),
red^{1} e^{1} ash2^{1}/TM6B, Tb^{1} (BL#4584),
w^{1118}; PBac{WH}Utx^{f01321}/CyO (BL#18425),
w; ash1^{22} P{FRT(w^{hs})}2A/TM6C, Sb^{1} Tb^{1}* (BL#24161),
w^{1118}; E(bx)$^{Nurf301-3}$/TM3, P{ActGFP}JMR2, Ser^{1} (BL#9687),
y^{1} w^{67c23}; P{lacW}Nurf-38^{k16102}/CyO (BL#12206),
Mi-2^{4} red^{1} e^{4}/TM6B, Sb^{1} Tb^{1} ca^{1} (BL#26170),
mor RNAi (VDRC#6969),
psq^{E39}/CyO; ry^{506} (BL#7321),

Rbf^{14} *w*^{1118}/*FM7c* (BL#7435),
w^{1118} *P{EP}Dsp1*^{EP355} (BL#17270),
cn^{1} *grh*^{IM} *bw*^{1}/*SM6a* (BL#3270),
y^{1} *w*^{67c23}; *P{lacW}lolal*^{k02512}/*CyO* (BL#10515),
w*; *P{neoFRT}42D Pcl*^{5}/*CyO* (BL#24157),
w*; *HDAC1*^{def24} *P{FRT(w*^{hs}*)}2A P{neoFRT}82B/TM6B, Tb*^{1} (BL#32239),
w^{1118}; *Sirt1*$^{2A-7-11}$ (BL#8838),
Eip74EF^{v4} *vtd*^{4}/*TM3, st*^{24} *Sb*^{1} (BL#5050),
sc^{1} *z*^{1} *w*^{is}; *Su(z)2*$^{1.b7}$/*CyO* (BL#5572),
P{PZ}gpp^{03342} *ry*^{506}/*TM3, ry*^{RK} *Sb*^{1} *Ser*^{1} (BL#11585),
y^{1} *w*^{1118}; *P{lacW}mod(mdg4)*^{L3101}/*TM3, Ser*^{1} (BL#10312),
w^{1118}; *PBac{RB}su(Hw)*^{e04061}/*TM6B, Tb*^{1} (BL#18224),
cn^{1} *P{PZ}lid*^{10424}/*CyO; ry*^{506} (BL#12367),
Asx^{XF23}/*CyO* (BL#6041),
y^{1} *w*^{1}; *P{neoFRT}40A P{FRT(w*^{hs}*)}G13*
cn^{1} *PBac{SAstopDsRed}dom*^{LL05537} *bw*^{1}/*CyO, bw*^{1} (BL#34496),
cn^{1} *E(Pc)*^{1} *bw*^{1}/*SM5* (BL#3056),
kis^{1} *cn*^{1} *bw*^{1} *sp*^{1}/*SM6a* (BL#431),
kto^{1} *ca*^{1}/*TM6B, Tb*^{1} (BL#3618),
skd^{2}/*TM6C, cu*^{1} *Sb*^{1} *ca*^{1} (BL#5047).

Genetic screen

Mutants or RNAi lines were crossed to *w*^{1118};; *rnGAL4, UAS-rpr, tubGAL80*^{ts}/*TM6B, tubGAL80* flies. Controls were *w*^{1118} or the appropriate RNAi background line. Embryos were collected at room temperature on grape plates for 4 h in the dark, then kept at 18°C. Larvae were picked at 2 days after egg lay into standard Bloomington cornmeal media and kept at 18°C, 50 larvae in each vial, three vials per genotype per replicate. On day 7, tissue ablation was induced by placing the vials in a 30°C circulating water bath for 24 h. Then ablation was stopped by placing the vials in ice water for 60 s and returning them to 18 °C for regeneration. The regeneration index was calculated by summing the product of approximate wing size (0%, 25%, 50%, 75%, and 100%) and the corresponding percentage of wings for each wing size. The Δ Index was calculated by subtracting the regeneration index of the control from the regeneration index of the mutant or RNAi line.

To observe and quantify the patterning features and absolute wing size, adult wings that were 75% size or greater were mounted in Gary's Magic Mount [Canada balsam (Sigma) dissolved in methyl salicylate (Sigma)]. The mounted adult wings were imaged with an Olympus SZX10 microscope using an Olympus DP21 camera, with the Olympus CellSens Dimension software. Wings were measured using ImageJ.

Immunostaining

Immunostaining was carried out as previously described (Smith-Bolton *et al.* 2009). Primary antibodies used in this study were rabbit anti-Myc (1:500; Santa Cruz Biotechnology), mouse anti-Nubbin (1:250; gift from Steve Cohen) (Ng *et al.* 1996), mouse anti-Engrailed/Invected [1:3; Developmental Studies Hybridoma Bank (DSHB)] (Patel *et al.* 1989), mouse anti-Patched (1:50; DSHB) (Capdevila *et al.* 1994), mouse anti-Achaete (1:10; DSHB) (Skeath and Carroll 1992), rabbit anti-PH3 (1:500; Millipore), mouse anti-Osa (1:1; DSHB) (Treisman *et al.* 1997), rat anti-Ci (1:10; DSHB) (Motzny and Holmgren 1995), rabbit anti-Dcp1 (1:250; Cell Signaling), mouse anti-βgal (1:100; DSHB), rabbit anti-phospho-Mad (1:100; Cell Signaling), mouse anti-Mmp1 (1:10 of 1:1:1 mixture of monoclonal antibodies 3B8D12, 5H7B11, and 3A6B4, DSHB) (Page-McCaw *et al.* 2003). The Developmental Studies Hybridoma Bank (DSHB) was created by the NICHD of the NIH and is maintained at the University of Iowa, Department of Biology, Iowa City, IA 52242, USA. Secondary antibodies used in this study were AlexaFluor secondary antibodies (Molecular Probes) (1:1000). TO-PRO-3 iodide (Molecular Probes) was used to detect DNA at 1:500.

Confocal images were collected with a Zeiss LSM700 Confocal Microscope using ZEN software (Zeiss). Images were processed with ImageJ (NIH) and Photoshop (Adobe). Average fluorescence intensity was measured by ImageJ. Quantification of fluorescence intensity and phospho-histone H3 positive cells was restricted to the wing pouch, as marked by anti-Nubbin immunostaining or morphology. The area of the regenerating wing primordium was quantified by measuring the anti-Nubbin immunostained area in ImageJ.

Quantitative RT-PCR

qPCR was conducted as previously described (Skinner *et al.* 2015). Each independent sample consisted of 50 wing discs. Three biological replicates were collected for each genotype and time point. Expression levels were normalized to the control *Gapdh2*. The fold changes compared to the *w*^{1118} undamaged wing discs are shown. Primers used in the study were:

Gapdh2 (Forward: 5′-GTGAAGCTGATCTCTTGGTACGAC-3′;
Reverse: 5′-CCGCGCCCTAATCTTTAACTTTTAC-3′),
ilp8 (Qiagen QT00510552),
mmp1 (Forward: 5′-TCGGCTGCAAGAACACGCCC-3′;
Reverse: 5′-CGCCCACGGCTGCGTCAAAG-3′),
moira (Forward: 5′-GATGAGGTGCCCGCTACAAT-3′;
Reverse: 5′-CTGCTGCGGTTTCGTCTTTT-3′),
brm (Forward: 5′-GCACCACCAGGGGATGATTT-3′;
Reverse: 5′-TTGTGTGGGTGCATTGGGT-3′),
Bap60 (Forward: 5′-AGACGAGGGATTTGAAGCTGA-3′;
Reverse: 5′-AGGTCTCTTGACGGTGGACT-3′)
Myc (Forward: 5′-CGATCGCAGACGACAGATAA-3′;
Reverse: 5′-GGGCGGTATTAAATGGACCT-3′)

Pupariation timing experiments

To quantify the pupariation rates, pupal cases on the side of each vial were counted at 24-h intervals starting from the end of tissue ablation until no new pupal cases formed. Three independent biological replicates, which consisted of three vials each with 50 animals per vial, were performed for each experiment. The median day is the day on which ≥50% of the animals had pupariated.

Data availability

All relevant data are available at https://doi.org/10.13012/B2IDB-1681718_V1 and upon request. Supplemental Material available at figshare: https://doi.org/10.25386/genetics.13260266.

Results

A genetic screen of chromatin modifier mutants and RNAi lines

To identify regeneration genes among *Drosophila* chromatin regulators, we conducted a genetic screen similar to our previously reported unbiased genetic screen for genes that regulate wing imaginal disc regeneration (Brock *et al.* 2017) (Figure 1A). To induce tissue ablation, *rotund-GAL4* drove the expression of the pro-apoptotic gene *reaper* via UAS control in the imaginal wing pouch, and *tubulin-GAL80*^{ts} provided temporal control, enabling us to turn ablation on and off by varying the temperature (Smith-Bolton *et al.* 2009). The ablation was carried out for 24 h

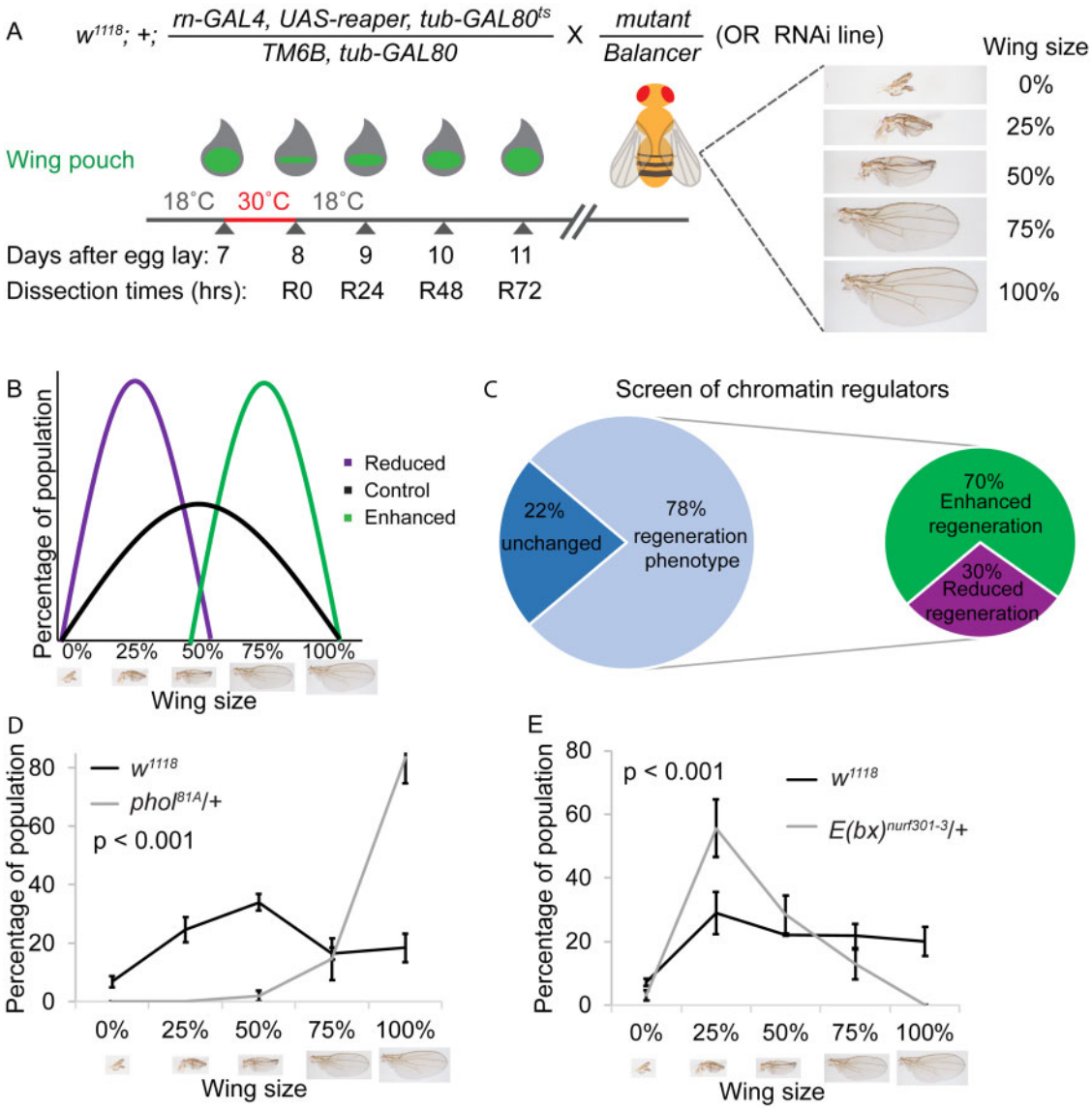

Figure 1 A genetic screen of chromatin regulators identified important regeneration genes. (A) Method for screening mutants or RNAi lines using a genetic ablation system. Mutants or RNAi lines of genes involved in regulating chromatin were crossed to the ablation stock (w^{1118}; +; *rn-GAL4, UAS-rpr, tubGAL80^{ts}/TM6B, tubGAL80*). Animals were kept at 18°C until 7 days after egg lay (AEL), when they were moved to 30°C to induce tissue ablation for 24 h, then transferred back to 18°C to enable recovery (R). The size of the regenerated adult wings was assessed semi-quantitatively by counting the number of wings that were approximately 0%, 25%, 50%, 75%, or 100% of the length of a control adult wing that had not undergone damage during the larval phase. The regenerating discs were also examined at different times denoted by hours after the beginning of recovery, such as R0, R24, R48, and R72. (B) Conceptual model for the screen to identify mutants or RNAi lines showing enhanced (green) or reduced (purple) regeneration compared to control. (C) Summary of the screen of chromatin regulators, showing percent of lines tested that had a regeneration phenotype, as well as percent of those with a phenotype that regenerated better (Δ Index $\geq$ 10%) or worse (Δ Index ≤ -10%) compared to controls. (D) Comparison of the size of adult wings after imaginal disc damage and regeneration in *phol*^{81A}/+ and wild-type (w^{1118}) animals. $n = 64$ wings (*phol*^{81A}/+) and 242 wings (w^{1118}) from three independent experiments. Chi-square test $P < 0.001$ across all wing sizes. Error bars are SEM. (E) Comparison of the size of adult wings after imaginal disc damage and regeneration in *E(bx)*$^{nurf301\text{-}3}$/+ and wild-type (w^{1118}) animals. $n = 219$ wings (*E(bx)*$^{nurf301\text{-}3}$/+) and 295 wings (w^{1118}) from three independent experiments. Chi-square test $P < 0.001$ across all wing sizes. Error bars are SEM.

during the early third instar. We characterized the quality of regeneration by assessing the adult wing size semi-quantitatively and (1) recording the numbers of wings that were 0%, 25%, 50%, 75%, or 100% the length of a normal adult wing (Figure 1, A and B), and (2) identifying patterning defects by scoring ectopic or missing features. This semi-quantitative evaluation method enabled a quick screen, at a rate of six genotypes per week including around 1400 adult wings, and identification of both enhancers and suppressors of regeneration (Figure 1, B–E). While control animals regenerated to varying degrees depending on the extent they delayed metamorphosis in response to damage (Smith-Bolton *et al.* 2009; Khan *et al.* 2017) as well as seasonal differences in humidity and food quality (Skinner *et al.* 2015), the differences between the regenerative capacity of mutants and controls were consistent (Smith-Bolton *et al.* 2009; Brock *et al.* 2017; Khan *et al.* 2017).

Using this system, we screened mutants and RNAi lines affecting chromatin regulators (Supplementary Table S1, Figure 1C, Supplementary Figure S1A). For each line, we calculated the Δ regeneration index, which is the difference between the regeneration indices of the line being tested and the control tested simultaneously (see *Materials and Methods* for regeneration index

calculation). We set a cutoff Δ index of 10%, over which we considered the regenerative capacity to be affected. Seventy-eight percent of the mutants and RNAi lines tested had a change in regeneration index of 10% or more compared to controls (Supplementary Table S1, Figure 1C, Supplementary Figure S1A), consistent with the idea that changes in chromatin structure are required for the damaged tissue to execute the regeneration program. Twenty-two percent of the mutants and RNAi lines failed to meet our cutoff and were not pursued further (Supplementary Table S1, Figure 1C). Strikingly, 53% of the tested lines, such as $phol^{81A}$/+, which affects the PhoRC complex, had larger adult wings after ablation and regeneration compared to control w^{1118} animals that had also regenerated (Figure 1D), indicating enhanced regeneration, although none were larger than a normal-sized wing. By contrast, 25% of the tested lines, such as $E(bx)^{nurf301\text{-}3}$/+, which affects the NURF complex, had smaller wings (Figure 1E), indicating worse regeneration. Unexpectedly, mutations that affected the same complex did not have consistent phenotypes (Supplementary Table S1), suggesting that chromatin modification and remodeling likely regulate a delicate balance of genes that promote and constrain regeneration. Indeed, transcriptional profiling has identified a subset of genes that are upregulated after wing disc ablation (Khan *et al.* 2017), some of which promote regeneration, and some of which constrain regeneration, indicating that gene regulation after tissue damage is not as simple as turning on genes that promote regeneration and turning off genes that inhibit regeneration.

The SWI/SNF PBAP and BAP complexes have opposite phenotypes

To clarify the roles of one type of chromatin-regulating complex in regeneration, we focused on the SWI/SNF chromatin-remodeling complexes (Figure 2A). As shown in Supplementary Table S1, different components of the SWI/SNF complexes showed different phenotypes after ablation and regeneration of the wing pouches. Animals heterozygous mutant for the PBAP-specific components Bap170 ($Bap170^{\Delta 135}$/+) and Polybromo ($polybromo^{\Delta 86}$/+) had adult wings that were smaller after disc regeneration than w^{1118} adult wings after disc regeneration (Figure 2, B and C), suggesting that the PBAP complex is required for ablated wing discs to regrow. To confirm these semiquantitative results, we mounted adult wings and measured absolute wing sizes ($N \geq 100$ wings for each genotype). The reduced regeneration of $Bap170^{\Delta 135}$/+ wing discs was confirmed by measurement of the adult wings, while adult $Bap170^{\Delta 135}$/+ wings without damage and regeneration in the discs were comparable to controls (Figure 2E, Supplementary Figure S1, B and D). By contrast, animals heterozygous mutant for the BAP-specific component Osa (osa^{308}/+) had larger adult wings after disc regeneration compared to w^{1118} adult wings after disc regeneration (Figure 2D), suggesting that impairment of the BAP complex deregulates growth after tissue damage. Measurement of the adult wings of osa^{308}/+ animals after disc regeneration confirmed the enhanced regeneration, while adult osa^{308}/+ wings without damage and regeneration in the discs were only slightly larger than controls (Figure 2F, Supplementary Figure S1, C and D).

Interestingly, the osa^{308}/+ adult wings also showed severe patterning defects after damage and regeneration of the disc (Figure 2, G–I). Specifically, the posterior compartment of the osa^{308}/+ wings had anterior features after wing pouch ablation, but had normal wings when no tissue damage was induced (Supplementary Figure S1C). To quantify the extent of the posterior-to-anterior (P-to-A) transformations, we quantified the number of anterior features in the posterior of each wing, including socketed bristles and ectopic veins on the posterior margin, an ectopic anterior crossvein (ACV), costal bristles on the alula, and an altered shape that has a narrower proximal and wider distal P compartment (Schuster and Smith-Bolton 2015) (Figure 2I). While w^{1118} adult wings that had regenerated as discs had a low level of P-to-A transformations, 75% of the osa^{308}/+ wings had P-to-A transformations, and 83% of these transformed wings had four or five anterior markers in the posterior of the wing. To confirm the phenotype, we tested an additional allele of *osa* and two deficiencies that remove the *osa* locus, all of which showed transformations of the posterior of the wing to anterior structures after damage and regeneration of the disc in heterozygous mutants (Supplementary Figure S1, E–H). Thus, Osa is required to preserve posterior cell fate during regeneration, suggesting that the BAP complex regulates cell fate after damage.

Reducing the core SWI/SNF components to varying levels produces either the BAP or PBAP phenotype

Because mutants of the BAP or PBAP complex-specific components showed distinct phenotypes, we also screened mutants of the core components for regeneration phenotypes. Interestingly, mutants or RNAi lines that reduced levels of the core components were split between the two phenotypes. For example, brm^2/+ discs and discs expressing a *Bap111* RNAi construct regenerated poorly, resulting in small wings (Figure 3, A and B), while $Bap55^{LL05955}$/+ discs, mor^1/+ discs, and discs expressing a *Bap60* RNAi construct regenerated to produce larger wings overall that showed P-to-A transformations (Supplementary Table S1, Figure 3, C–G, , Supplementary Figure S1A).

Given that the SWI/SNF complexes require the function of the scaffold Mor and the ATPase Brm (Moshkin *et al.* 2007; Mashtalir *et al.* 2018), it was surprising that reduction of Mor showed the BAP phenotype while reduction of Brm showed the PBAP phenotype. However, it is likely that some of the mutants and RNAi lines caused stronger loss of function than others, due to strength of the allele or the transient and localized nature of RNAi. A stronger reduction in function would result in malfunction of both BAP and PBAP, and show the reduced regeneration phenotype, masking any patterning defects. By contrast, a weaker or transient reduction in function could mainly affect the BAP complex. For example, *Bap60* RNAi, which caused patterning defects after wing disc regeneration, only induced a moderate reduction in mRNA levels, suggesting that it causes a weak loss of function (Supplementary Figure S2A). Although it is unclear why a weaker reduction of function would mainly affect the BAP complex, it is possible that the BAP complex is less abundant than the PBAP complex, such that a slight reduction in a core component would have a greater effect on the amount of BAP in the tissue. Therefore, we hypothesized that stronger or weaker loss of function of the same core complex component might show different phenotypes.

To test this hypothesis, we used a strong loss-of-function *mor* mutant, mor^{11} (gift from J. Kennison, Supplementary Figure S2B), and two hypomorphic *mor* mutants mor^1 *and* mor^2 (Kennison and Tamkun 1988). Indeed, mor^{11}/+ undamaged wing discs had significantly less *mor* transcript than mor^1/+ or control undamaged wing discs (Figure 3H). Interestingly, mor^{11}/+ animals showed the poor regeneration phenotype similar to the PBAP complex-specific $Bap170^{\Delta 135}$/+ mutants (Figure 3I), while mor^1/+ and mor^2/+ showed the enhanced regeneration phenotype and the P-to-A transformation phenotype similar to the BAP complex-specific

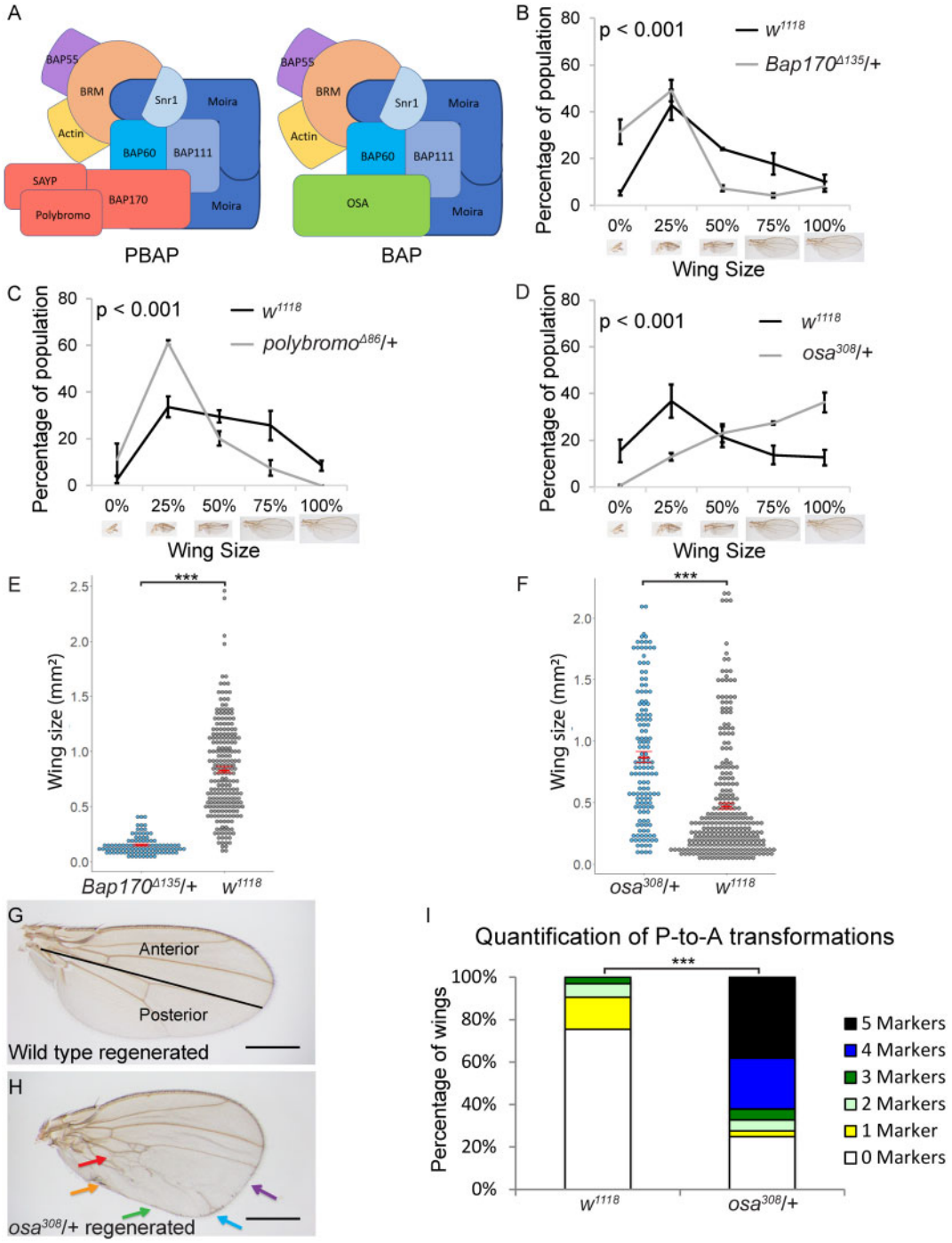

Figure 2 SWI/SNF components Bap170, Polybromo and Osa are required for regeneration. (A) Schematics of the two *Drosophila* SWI/SNF chromatin-remodeling complexes: BAP and PBAP, drawn based on complex organization determined in (Mashtalir *et al.* 2018). (B) Comparison of the size of adult wings after imaginal disc damage and regeneration in $Bap170^{\Delta135}$/+ and wild-type (w^{1118}) animals. $n = 190$ wings ($Bap170^{\Delta135}$/+) and 406 wings (w^{1118}) from three independent experiments. Chi-square test $P < 0.001$ across all wing sizes. (C) Comparison of the size of adult wings after imaginal disc damage and regeneration in $polybromo^{\Delta86}$/+ and wild-type (w^{1118}) animals. $n = 180$ wings ($polybromo^{\Delta86}$/+) and 396 wings (w^{1118}) from three independent experiments. Chi-square test $P < 0.001$ across all wing sizes. (D) Comparison of the size of adult wings after imaginal disc damage and regeneration in osa^{308}/+ and wild-type (w^{1118}) animals. $n = 146$ wings (osa^{308}/+) and 296 wings (w^{1118}) from three independent experiments. Chi-square test $P < 0.001$ across all wing sizes. (E) Wings were mounted, imaged, and measured after imaginal disc damage and regeneration in $Bap170^{\Delta135}$/+ and wild-type (w^{1118}) animals. $n = 100$ wings ($Bap170^{\Delta135}$/+) and 224 wings (w^{1118}) from three independent experiments. Student's *t*-test, $P < 0.001$. (F) Wings were mounted, imaged, and measured after imaginal disc damage and regeneration in osa^{308}/+ and wild-type (w^{1118}) animals. $n = 142$ wings (osa^{308}/+) and 284 wings (w^{1118}) from three independent experiments. (G) Wild-type (w^{1118}) adult wing after disc regeneration. Anterior is up. (H) osa^{308}/+ adult wing after disc regeneration. Arrows show five anterior-specific markers in the posterior compartment: anterior crossveins (red), alula-like costa bristles (orange), margin vein (green), socketed bristles (blue), and change of wing shape with wider distal portion of the wing, similar to the anterior compartment (purple). (I) Quantification of the number of Posterior-to-Anterior transformation markers described in (H) in each wing after damage and regeneration of the disc, using wings that were 75% normal size or larger, comparing osa^{308}/+ wings to wild-type (w^{1118}) wings, $n = 51$ wings (osa^{308}/+) and 45 wings (w^{1118}), from three independent experiments. Chi-square test $P < 0.001$. Error bars are SEM. Scale bars are 500 μm for all adult wings images. *$P < 0.05$, **$P < 0.01$, ***$P < 0.001$ Student's *t*-test.

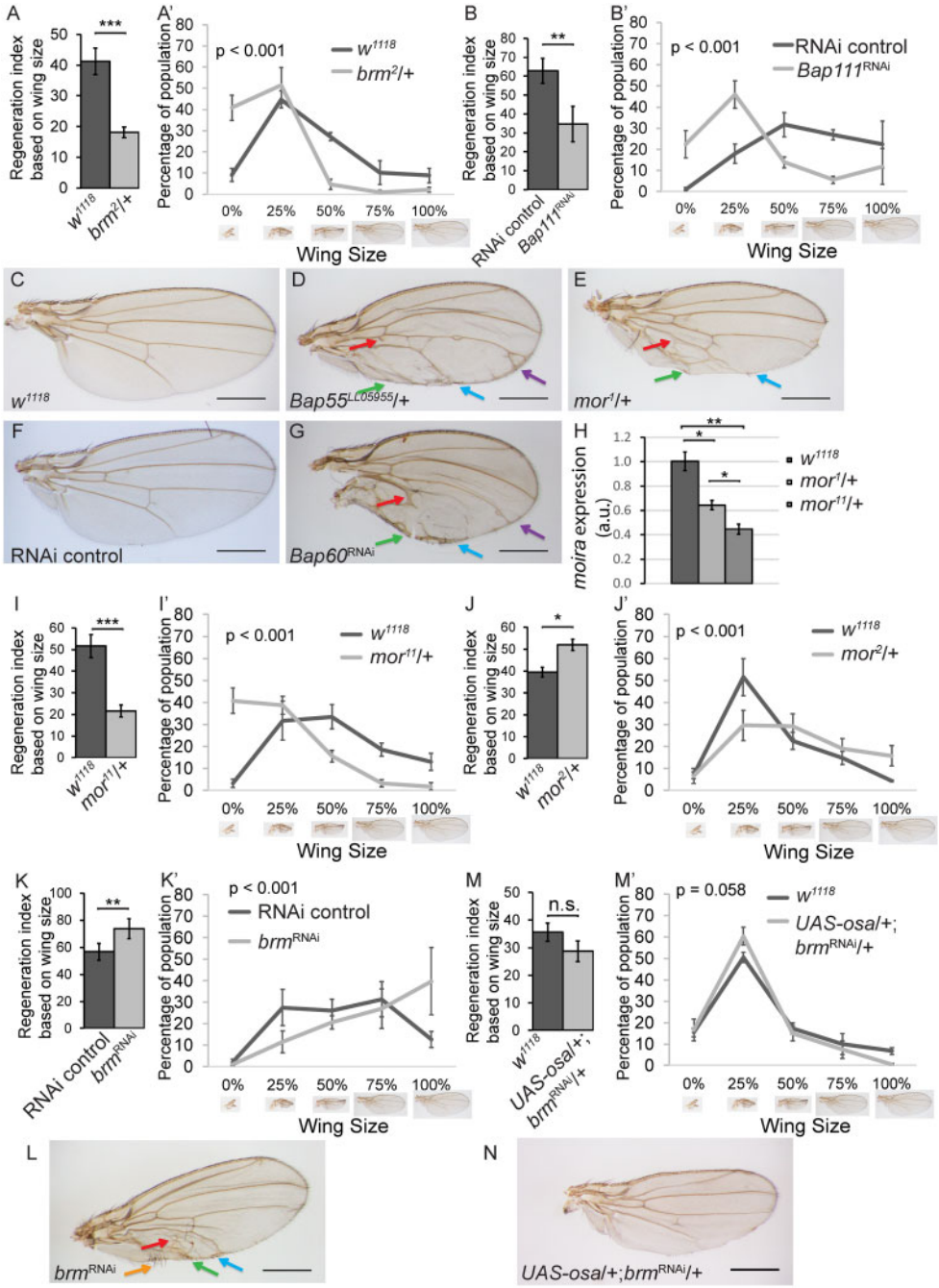

Figure 3 SWI/SNF core components are required for both growth and posterior fate during wing disc regeneration. (A) Comparison of the size of adult wings after imaginal disc damage and regeneration in brm^2/+ and wild-type (w^{1118}) animals. $n = 142$ wings (brm^2/+) and 224 wings (w^{1118}) from three independent experiments, student's *t*-test $P < 0.001$. (A′) Chi-square test $P < 0.001$ across all wing sizes. (B) Comparison of the size of adult wings after imaginal disc damage and regeneration in animals expressing *Bap111* RNAi and control animals. $n = 264$ wings (*Bap111* RNAi) and 291 wings (control) from three independent experiments. The control for RNAi lines is VDRC 15293 in all experiments, student's *t*-test $P < 0.01$. (B′) Chi-square test $P < 0.001$ across all wing sizes. (C–G) Adult wing after disc regeneration of wild-type (w^{1118}) (C), $Bap55^{LL05955}$/+ (D), mor^1/+ (E), RNAi control (F) or *Bap60* RNAi (G). Anterior is up for all adult wing images. Arrows point to anterior features identified in the posterior compartment. Arrows show five anterior-specific markers in the posterior compartment: anterior cross veins (red), alula-like costa bristles (orange), margin vein (green), socketed bristles (blue), and change of wing shape with wider distal portion of the wing, similar to the anterior compartment (purple). (H) *moira* expression determined by qPCR of mor^1/+, mor^{11}/+ and wild-type (w^{1118}) undamaged wing discs at R24. The graph shows fold change relative to wild-type (w^{1118}) discs. (I) Comparison of the size of adult wings after imaginal disc damage and regeneration in mor^{11}/+ and wild-type (w^{1118}) animals. $n = 114$ wings (mor^{11}/+) and 328 wings (w^{1118}) from three independent experiments, student's *t*-test $P < 0.001$. (I′) Chi-square test $P < 0.001$ across all wing sizes. (J) Comparison of the size of adult wings after imaginal disc damage and regeneration in mor^2/+ and wild-type (w^{1118}) animals. $n = 134$ wings (mor^2/+) and 414 wings (w^{1118}) from three independent experiments, student's *t*-test $P < 0.05$. (J′) Chi-square test $P < 0.001$ across all wing sizes. (K) Comparison of the size of adult wings after imaginal disc damage and regeneration in animals expressing *brm* RNAi and control animals. $n = 234$ wings (*brm* RNAi) and 281 wings (control) from three independent experiments, student's *t*-test $P < 0.01$. (K′) Chi-square test $P < 0.001$ across all wing sizes. (L) Adult wing after disc regeneration while expressing *brm* RNAi. (M) Comparison of the size of adult wings after imaginal disc damage and regeneration in *UAS-osa/+; brm* ^{RNAi}/+ and wild-type (w^{1118}) animals. $n = 117$ wings (*UAS-osa/+; brm* ^{RNAi}/+) and 348 wings (w^{1118}) from three independent experiments, student's *t*-test not significant. (M′) Chi-square test across all wing sizes $P = 0.058$, not significant at $\alpha = 0.05$ level. (N) Adult wing after imaginal disc regeneration in *UAS-osa/+; brm*^{RNAi}/+ animal. Error bars are SEM. Scale bars are 500 μm for all adult wing images. *$P < 0.05$, **$P < 0.01$, ***$P < 0.001$ Student's *t*-test.

osa^{308}/+ mutants (Figure 3, E and J, Supplementary Table S1). Importantly, both phenotypes were observed using mutant alleles, ruling out the possibility that one phenotype was the result of RNAi. To confirm these findings, we also used an amorphic allele of *brm* and an RNAi line that targets *brm* to reduce the levels of the core component *brm*. brm^2 was generated through ethyl methanesulfonate mutagenesis and causes a loss of Brm protein without affecting transcript levels (Kennison and Tamkun 1988; Elfring *et al.* 1998). The *brm* RNAi causes a partial reduction in transcript, as *rn>brmRNAi* undamaged wing discs had less *brm* transcript than control undamaged wing discs (Supplementary Figure S2C). brm^2/+ animals showed the small wing phenotype after disc damage, indicating poor regeneration (Figure 3A). By contrast, knockdown of *brm* by expressing the *brm* RNAi construct during tissue ablation induced larger wings and P-to-A transformations (Figure 3, K and L). Thus, slight reduction of the core SWI/SNF components, through mor^1, *brm* RNAi, or *Bap60* RNAi, produced the BAP phenotype, whereas stronger reduction of the core components, through mor^{11}, produced the PBAP phenotype, suggesting that it is easier to compromise BAP function than to compromise PBAP function. If it is easier to compromise BAP function because there is less BAP complex in regenerating wing disc cells, overexpression of the BAP-specific component Osa would lead to an increase in the amount of BAP complex and rescue the *brm* RNAi phenotype. Indeed, overexpression of *osa* in regenerating tissue rescued the enhanced wing size and P-to-A transformations induced by *brm* RNAi (Figure 3, M and N).

The PBAP complex is required for Myc upregulation and cell proliferation during regrowth

To identify when the defect in regrowth occurs in PBAP complex mutants, we measured the regenerating wing pouch using expression of the pouch marker *nubbin* in w^{1118} controls, $Bap170^{\Delta135}$/+ and brm^2/+ mutants, as well as in the osa^{308}/+ BAP mutant for comparison. The regenerating wing pouches of $Bap170^{\Delta135}$/+ mutant animals were not different in size compared to w^{1118} animals at 0, 12, or 24 h after tissue damage (R0, R12, or R24). However, the $Bap170^{\Delta135}$/+ regenerating wing pouches were smaller than w^{1118} by 36 hours after tissue damage (R36), shortly before the $Bap170^{\Delta135}$/+ mutant animals pupariated and entered metamorphosis (Figure 4, A–C). brm^2/+ mutant animals also had smaller regenerating wing pouches by R24 (Supplementary Figure S3, A–C). By contrast, the regenerating osa^{308}/+ wing pouches regrew at the same rate as controls (Supplementary Figure S3, D–H).

To determine whether the $Bap170^{\Delta135}$/+ mutant animals had a slower rate of proliferation during regeneration, we quantified the number of mitotic cells by immunostaining for phosphohistone H3 (PH3) in the regenerating wing pouch. A 35% decrease in the number of PH3-positive cells was observed in $Bap170^{\Delta135}$/+ mutants (Figure 4, D–F, Supplementary Figure S3I). Interestingly, there was also a slight but significant decrease in PH3-positive cells outside of the regenerating wing pouch in $Bap170^{\Delta135}$/+ mutants (Supplementary Figure S3J), although there was no difference in pouch size or PH3-positive cells within or outside the pouch in undamaged discs (Supplementary Figure S3, K–N). While smaller adult wings could also be caused by increased cell death in the regenerating tissue, we did not find an increase in cell death in $Bap170^{\Delta135}$/+ regenerating wing discs as marked by immunostaining for cleaved caspase Dcp1 (Supplementary Figure S3, O and P).

To identify why proliferation was reduced in $Bap170^{\Delta135}$/+ mutants, we examined levels of Myc, an important growth regulator that is upregulated during *Drosophila* wing disc regeneration (Smith-Bolton *et al.* 2009). In mammals, *c-myc* is a direct target of the SWI/SNF BAF complex, which is similar to *Drosophila* BAP (Nagl *et al.* 2006), but a role for the PBAP complex in regulating the *Drosophila Myc* gene has not been established. Myc protein levels were significantly reduced in $Bap170^{\Delta135}$/+ and brm^2/+ regenerating wing pouches compared to wild-type regenerating wing pouches (Figure 4, G-I and Supplementary Figure S4, A–D). *Myc* transcriptional levels were also significantly lower in $Bap170^{\Delta135}$/+ regenerating wing discs compared to wild-type regenerating discs (Figure 4J). By contrast, there was no change in Myc levels in osa^{308}/+ mutants (Supplementary Figure S4, E–G), indicating that upregulation of Myc after tissue damage is sensitive to reduction of PBAP, but not BAP. To determine the extent to which reduction of Myc expression was responsible for the poor regeneration phenotype in BAP complex mutants, we overexpressed Myc in the $Bap170^{\Delta135}$/+ background during regeneration. Indeed, the $Bap170^{\Delta135}$/+, *UAS-Myc*/+ animals regenerated similar to the w^{1118} controls and significantly better than $Bap170^{\Delta135}$/+ animals, demonstrating partial rescue of the poor regeneration phenotype (Figure 4K and Supplementary Figure S4H).

The PBAP complex is required for the delay in pupariation induced by tissue damage

Damaged imaginal discs delay pupariation by expressing the peptide ILP8, which delays the production of ecdysone and onset of metamorphosis, providing more time for damaged tissue to regenerate (Colombani *et al.* 2012; Garelli *et al.* 2012). To determine whether the SWI/SNF complexes regulate the timing of metamorphosis, we quantified the pupariation rate in w^{1118} and $Bap170^{\Delta135}$/+ regenerating animals, and identified the day on which 50% of the larvae had pupariated. Without tissue damage, $Bap170^{\Delta135}$/+ mutants pupariated slightly later than w^{1118} animals (Figure 4L and Supplementary Figure S5A), but the difference is not significant. However, after wing disc damage, more than half of the $Bap170^{\Delta135}$/+ mutant animals had pupariated by 2 days after damage, whereas more than half of the w^{1118} animals had not pupariated until 3 days after damage, giving the mutants 1/3 less time to regenerate (Figure 4M and Supplementary Figure S5B). To uncover why $Bap170^{\Delta135}$/+ animals had less regeneration time, we quantified *ilp8* transcript levels. Indeed, $Bap170^{\Delta135}$/+ animals had about 50% less *ilp8* mRNA (Figure 4N), suggesting that the PBAP complex is required for *ilp8* expression.

The PBAP complex regulates expression of JNK signaling targets

SWI/SNF complexes can be recruited by transcription factors to act as co-activators of gene expression (Becker and Workman 2013). Regenerative growth and the pupariation delay are regulated by JNK signaling (Bosch *et al.* 2008; Bergantinos *et al.* 2010; Colombani *et al.* 2012; Garelli *et al.* 2012; Skinner *et al.* 2015). Thus, it is possible that PBAP is recruited to JNK signaling targets like *ilp8* by the AP-1 transcription factor, which acts downstream of JNK (Perkins *et al.* 1988), and that PBAP is required for full activation of these targets. To determine whether *Bap170* is required for JNK-dependent transcription, we examined the activity of the *TRE-Red* reporter, which is comprised of four AP-1 binding sites (TREs) driving the expression of a *DsRed.T4* reporter gene (Chatterjee and Bohmann 2012) in w^{1118} and $Bap170^{\Delta135}$/+ regenerating wing discs. The TRE-Red intensity was

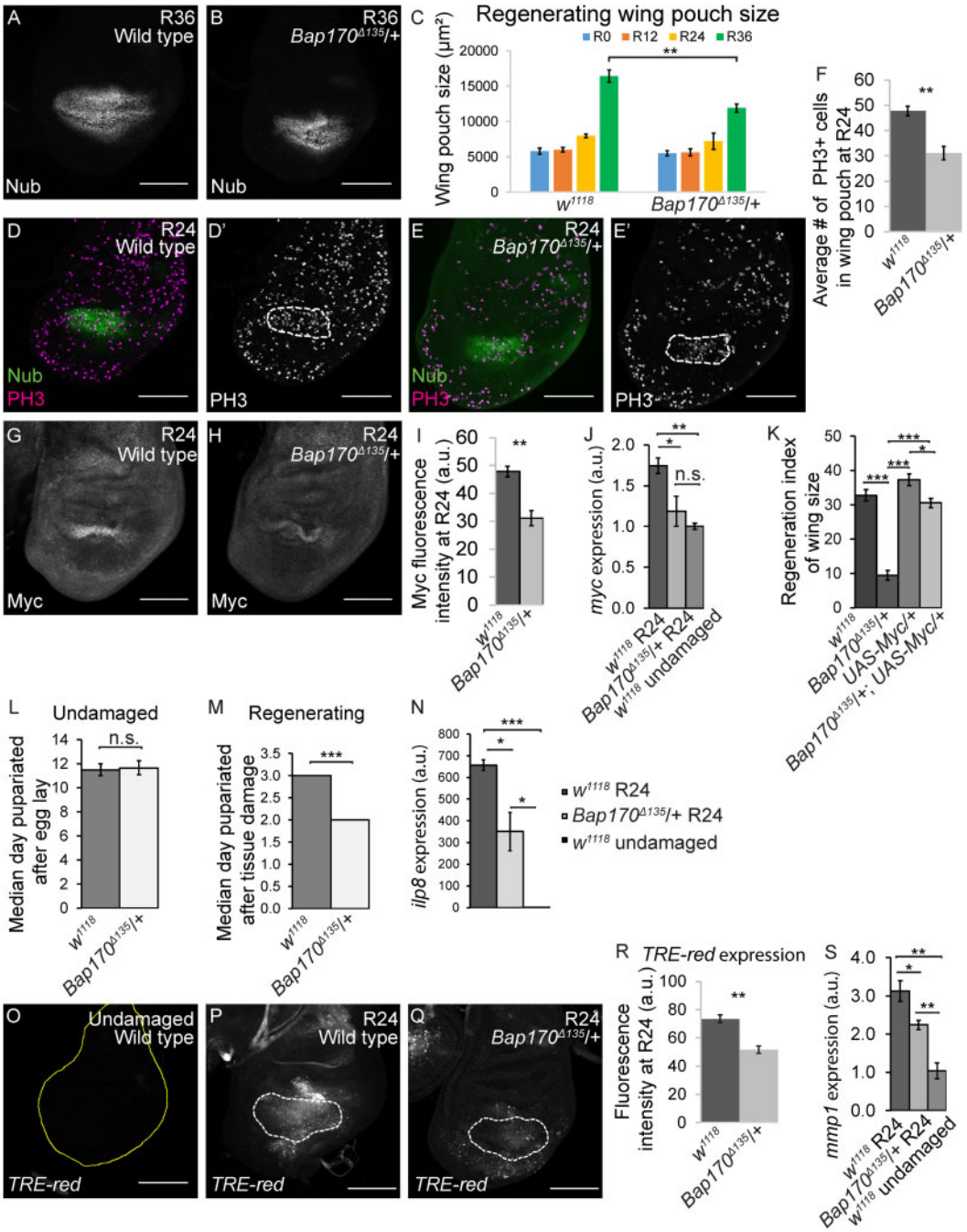

Figure 4 Decreased *Bap170* expression limits regenerative growth and pupariation delay. (A) Wild-type (w^{1118}) regenerating wing disc at R36 with wing pouch marked by anti-Nubbin (green) immunostaining. (B) $Bap170^{\Delta135}$/+ regenerating wing disc at R36 with wing pouch marked by anti-Nubbin (green) immunostaining. (C) Comparison of regenerating wing pouch size at 0, 12, 24, and 36 h after imaginal disc damage in $Bap170^{\Delta135}$/+ and wild-type (w^{1118}) animals. (D, E) Regenerating wild-type (w^{1118}) (D) and $Bap170^{\Delta135}$/+ (E) wing discs at R24 with Nubbin (green) and PH3 (magenta) immunostaining. Dashed white outline shows the regenerating wing primordium labeled with Nubbin. (F) Average number of mitotic cells (marked with PH3 immunostaining) in the wing primordium (marked by anti-Nubbin) at R24 in $Bap170^{\Delta135}$/+ and wild-type (w^{1118}) animals. $n = 8$ wing discs ($Bap170^{\Delta135}$/+) and 10 wing discs (w^{1118}). (G-H) Wild-type (w^{1118}) (G) and $Bap170^{\Delta135}$/+ (H) regenerating wing discs at R24 with Myc immunostaining. (I) Quantification of anti-Myc immunostaining fluorescence intensity in the wing pouch in $Bap170^{\Delta135}$/+ and wild-type (w^{1118}) regenerating wing discs at R24. $n = 9$ wing discs ($Bap170^{\Delta135}$/+) and 9 wing discs (w^{1118}). (L) Median time to pupariation for animals during normal development at 18°C. $n = 103$ pupae ($Bap170^{\Delta135}$/+) and 227 pupae (w^{1118}) from three independent experiments. Student's *t*-test not significant. (M) Median time to pupariation for animals after tissue damage (30°C) and regeneration (18°C). $n = 117$ pupae ($Bap170^{\Delta135}$/+) and 231 pupae (w^{1118}) from three independent experiments. Because the temperature shift to 30°C in the ablation protocol increases the developmental rate, the pupariation timing of regenerating animals (M) cannot be compared to the undamaged control animals (L). Student's *t*-test $P < 0.001$. (N) *ilp8* expression examined by qPCR of $Bap170^{\Delta135}$/+ and wild-type (w^{1118}) regenerating wing discs at R24. The graph shows fold change relative to wild-type (w^{1118}) undamaged discs. (O–Q) Expression of *TRE-Red*, a JNK signaling reporter, in wild-type (w^{1118}) undamaged (O), as well as wild-type (w^{1118}) (P) and $Bap170^{\Delta135}$/+ (Q) regenerating wing discs at R24. Yellow outline shows the wing disc in (O). White dashed lines show the wing pouch in (P) and (Q) as marked by anti-Nub. (R) Quantification of *TRE-Red* fluorescence intensity in $Bap170^{\Delta135}$/+ and wild-type (w^{1118}) regenerating wing pouches at R24. $n = 12$ wing discs ($Bap170^{\Delta135}$/+) and 14 wing discs (w^{1118}). (S) *mmp1* expression examined by qPCR of wild-type (w^{1118}) and $Bap170^{\Delta135}$/+ regenerating wing discs at R24, and wild-type (w^{1118}) undamaged discs. The graph shows fold change relative to wild-type (w^{1118}) regenerating discs at R24. Scale bars are 100μm for all wing discs images. *$P < 0.05$, **$P < 0.01$, ***$P < 0.001$, Student's *t*-test.

significantly decreased in the *Bap170*$^{\Delta 135}$/+ regenerating tissue compared to the *w*^{1118} regenerating tissue (Figure 4, O–R), indicating that PBAP is required for full activation of this AP-1 transcriptional activity reporter, similar to its requirement for expression of *ilp8*. Furthermore, expression of the JNK signaling target *matrix metalloproteinase 1 (mmp1)* was significantly reduced in *Bap170*$^{\Delta 135}$/+ regenerating wing discs at both the mRNA and protein levels (Figure 4S and Supplementary Figure S5, C–E). Thus, the PBAP complex plays a crucial role in the activation of JNK signaling targets.

The BAP complex maintains posterior cell fate during regeneration

After damage and regeneration of the disc, adult wings of *osa*^{308}/+, *Bap55*^{LL05955}/+, *mor*^{1}/+, and *mor*^{2}/+ discs, as well as discs expressing a *brm* RNAi construct or a *Bap60* RNAi construct, had anterior bristles and veins in the posterior compartment (Figure 3, C–-G and K), but not after normal development (Supplementary Figures S1A and S2, D–F). To identify when the P-to-A transformations occurred, we examined the expression of anterior- and posterior-specific genes during tissue regeneration.

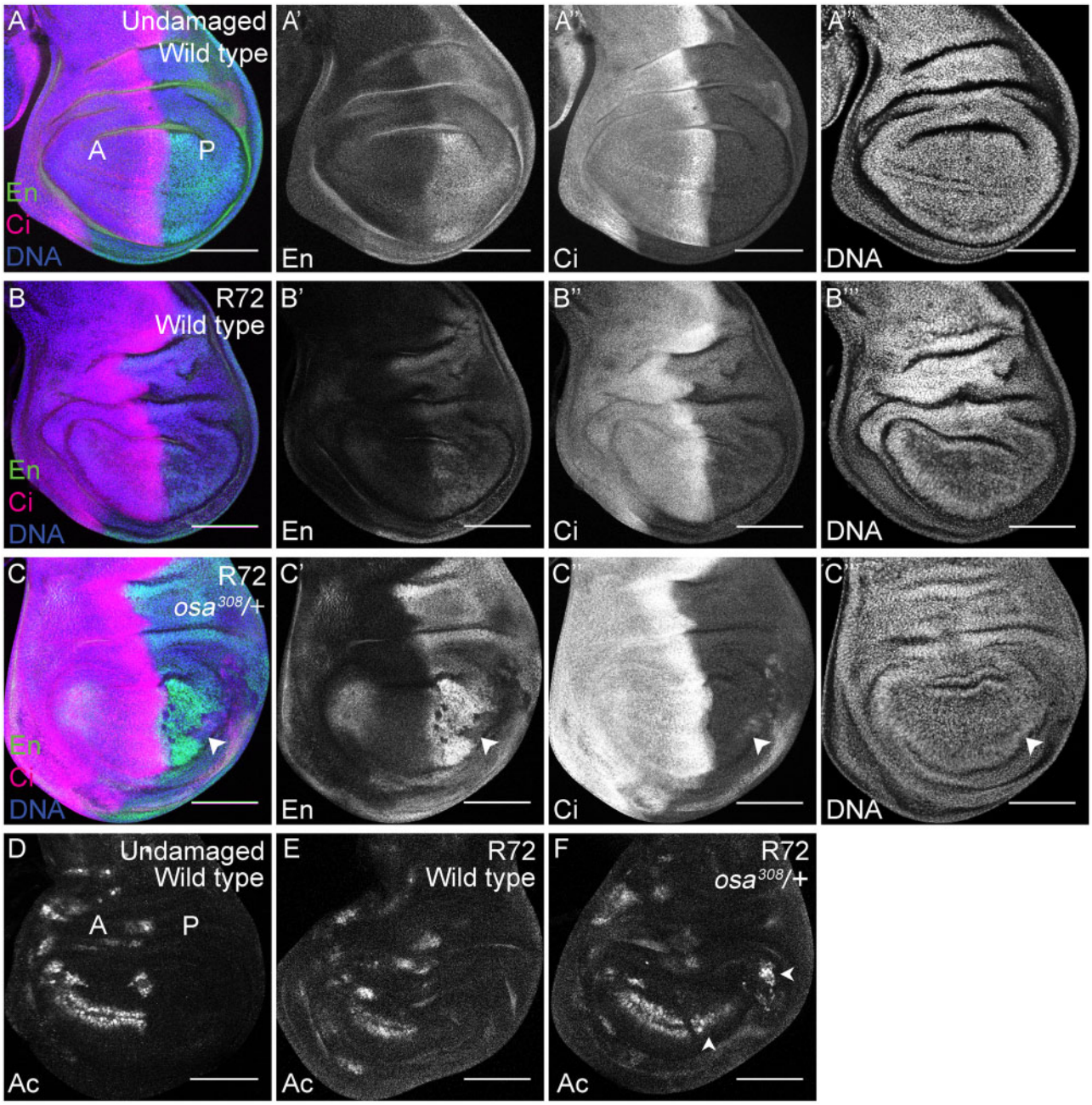

Figure 5 Reduction of Osa causes Posterior-to-Anterior transformations during wing disc regeneration. (A) Wild-type (*w*^{1118}) undamaged wing disc with En (green) (A′) and Ci (magenta) (A″) immunostaining. DNA (blue) (A‴) was detected with Topro3 here and in subsequent panels. Anterior is left for all wing disc images. (B) Wild-type (*w*^{1118}) regenerating wing disc at R72 with En (green) (B′) and Ci (magenta) (B″) immunostaining and DNA (blue) (B‴). (C) *osa*^{308}/+ regenerating wing disc at R72 with En (green) (C′) and Ci (magenta) (C″) immunostaining, and DNA (blue) (C‴). Arrowhead points to the low En expression region in which Ci is expressed in the posterior compartment. (D) Wild-type (*w*^{1118}) undamaged wing disc with Ac immunostaining. (E) Wild-type (*w*^{1118}) regenerating wing disc at R72 with Ac immunostaining. (F) *osa*^{308}/+ regenerating wing disc at R72 with Ac immunostaining. Arrowheads show Ac expression in the posterior compartment. Scale bars are 100μm for all wing discs images.

engrailed (*en*) is essential for posterior cell fate both in development and regeneration (Kornberg *et al.* 1985; Schuster and Smith-Bolton 2015). To assess ability to maintain posterior cell fate, regenerating wing discs were dissected at different times during recovery (R) and immunostained for the posterior selector gene *en*. At 72 hours after damage (R72), in osa^{308}/+ regenerating discs, *en* was expressed in some of the posterior compartment, but lost in patches (Figure 5, A–C). In addition, the proneural protein Acheate (Ac), which is expressed in sensory organ precursors in the anterior of wing discs (Skeath and Carroll 1991), was ectopically expressed in the posterior (Figure 5, D–F) marking precursors to the ectopic socketed bristles found in the posterior of the adult wings. The anterior genes *cubitus interruptus* (*ci*) (Eaton and Kornberg 1990) and *patched* (*ptc*) (Phillips *et al.* 1990) were also ectopically expressed in the posterior of the osa^{308}/+ R72 regenerating wing discs but not in undamaged osa^{308}/+ wing discs (Figure 6, A–C, Supplementary S5, F and G). The ectopic expression of these anterior genes was not observed at R48, suggesting that the P-to-A fate transformations happened late during regeneration (Supplementary Figure S5, H and I). Similarly, at R72, 80% of the *brm* RNAi wing discs had ectopic expression of the anterior genes *ptc* and *ci* in the posterior of the discs, while no expression of *ptc* or *ci* was observed in the posterior of control R72 discs (Figure 6, D and E).

We previously showed that in *Drosophila* wing disc regeneration, elevated JNK increases expression of *en*, leading to PRC2-mediated silencing of the *en* locus in patches, and transformation of the *en*-silenced cells to anterior fate, and that Taranis (Tara) prevents this misregulation of *en* and resulting P-to-A cell fate transformations (Schuster and Smith-Bolton 2015). Thus, we wondered whether the BAP complex preserved *en* expression and posterior fate by reducing JNK signaling, or regulating *tara* expression, or working in parallel to Tara during the later stages of regeneration.

The BAP complex does not regulate JNK signaling

To determine whether the BAP complex regulates JNK signaling, we examined the JNK reporter *TRE-Red* in osa^{308}/+ and w^{1118} regenerating wing discs. In contrast to $Bap170^{\Delta 135}$/+ mutants (Figure 4, O–R), TRE-Red intensity was not different between osa^{308}/+ and w^{1118} regenerating tissue (Figure 7, A–C). Thus, the BAP complex acts to protect posterior cell fate downstream of or in parallel to JNK signaling.

The BAP complex functions in parallel to Taranis to preserve cell fate

Because *tara* is regulated transcriptionally after tissue damage (Schuster and Smith-Bolton 2015), we examined whether the BAP complex is required for *tara* upregulation in the regenerating tissue. Using a *tara-lacZ* enhancer trap, we assessed expression in $Bap55^{LL05955}$/+ regenerating wing discs, which had the same P-to-A transformations as the osa^{308}/+ regenerating discs. We used the $Bap55^{LL05955}$ allele instead of an *osa* allele for technical reasons, as our ablation system, *tara*, and *osa* are all on the third chromosome, and $Bap55^{LL05955}$ and *osa* alleles gave the same phenotype. No change in *tara-lacZ* expression was identified in the regenerating wing pouches (Figure 7, D–G), indicating that the damage-dependent *tara* expression was not downstream of BAP activity.

To determine whether Tara can suppress the P-to-A transformations induced by the reduction of BAP, we overexpressed Tara

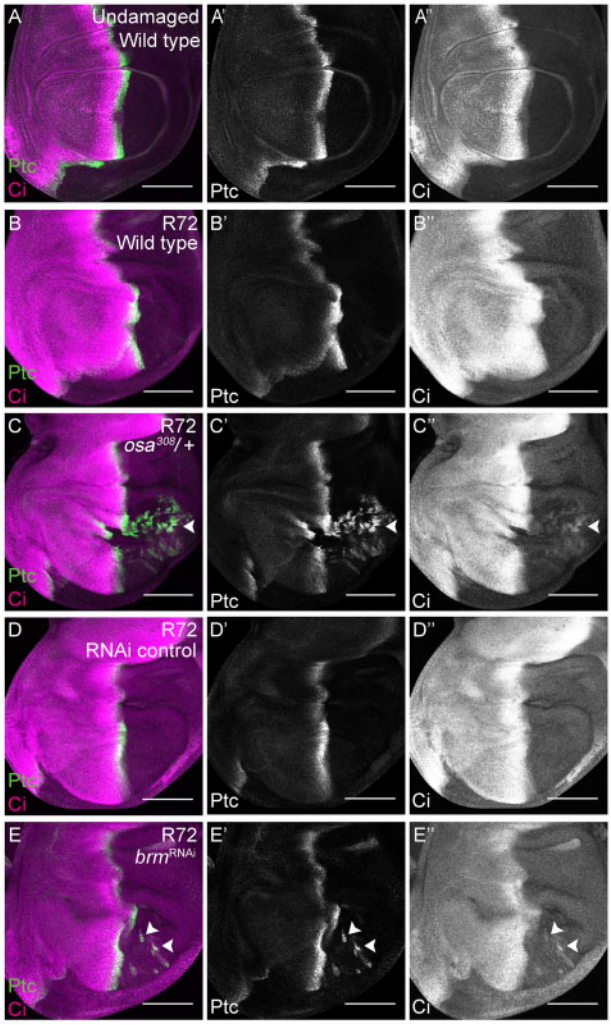

Figure 6 The BAP complex is required to maintain posterior cell fate during wing disc regeneration. (A) Wild-type (w^{1118}) undamaged wing disc with Ptc (green) (A′) and Ci (magenta) (A″) immunostaining. (B) Wild-type (w^{1118}) regenerating wing disc at R72 with Ptc (green) (B′) and Ci (magenta) (B″) immunostaining. (C) osa^{308}/+ regenerating wing disc at R72 with Ptc (green) (C′) and Ci (magenta) (C″) immunostaining. Arrowhead shows Ptc and Ci co-expression in the posterior compartment. (D) RNAi control regenerating wing disc at R72 with Ptc (green) (D′) and Ci (magenta) (D″) immunostaining. (E) Regenerating wing disc of animals expressing *brm* RNAi at R72 with Ptc (green) (E′) and Ci (magenta) (E″) immunostaining. Arrowheads show Ptc and Ci co-expression in the posterior compartment. Scale bars are 100 μm for all wing disc images.

using *UAS-tara* under control of *rn-Gal4* in the osa^{308}/+ mutant animals, generating elevated Tara levels in the *rn*-expressing cells that survived the tissue ablation. Indeed, the P-to-A transformation phenotype in osa^{308}/+ mutant animals was rescued by Tara overexpression (Figure 7, H–K). To rule out the possibility that Tara regulates *osa* expression, we quantified Osa immunostaining in *tara*/+ mutant regenerating tissue. Osa protein levels did not change during regeneration, and were unchanged in $tara^{1}$/+ mutant regenerating discs (Supplementary Figure S6, A–F). Taken together, these data indicate that the BAP complex likely functions in parallel to Tara to constrain *en* expression, preventing auto-regulation and silencing of *en*, thereby protecting cell fate from changes induced by JNK signaling during regeneration.

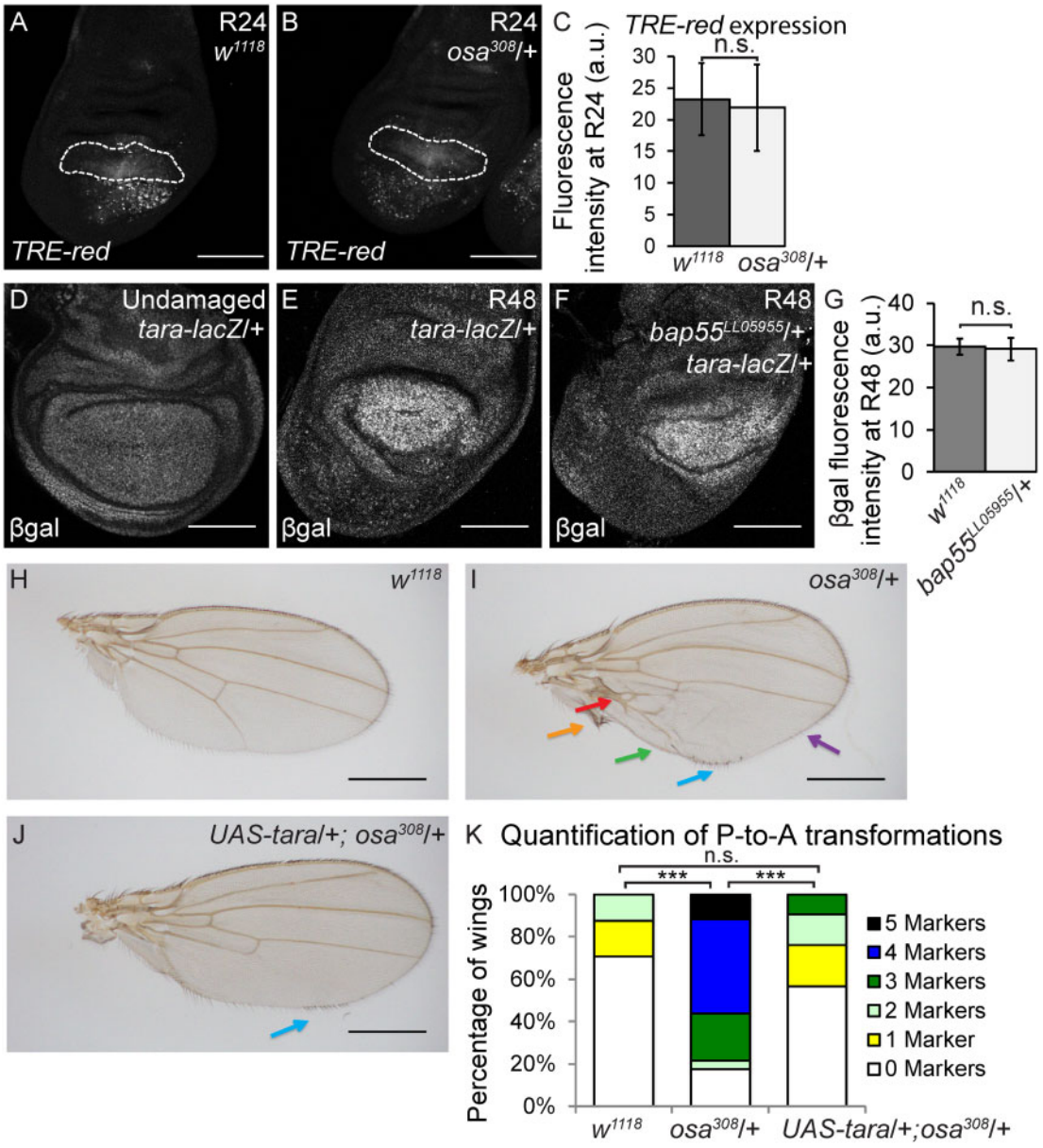

Figure 7 The BAP complex functions in parallel to Tara to prevent P-to-A transformations. (A-B) Expression of *TRE-Red*, a JNK signaling reporter, in wild-type (w^{1118}) (A) and osa^{308}/+ (B) regenerating wing discs at R24. Dashed white outline shows the regenerating wing primordium as marked by anti-Nub and excluding the debris field. (C) Quantification of *TRE-Red* expression fluorescence intensity in osa^{308}/+ and wild-type (w^{1118}) regenerating wing pouches at R24. $n = 26$ wing discs (osa^{308}/+) and 31 wing discs (w^{1118}). Error bars are SEM. (D–F) *tara* expression detected with anti- β-gal immunostaining in *tara-lacZ*/+ undamaged (D), *tara-lacZ*/+ R48 (E) and $Bap55^{LL05955}$/+; *tara-lacZ*/+ R48 (F) regenerating wing discs. (G) Quantification of β-gal expression via fluorescence intensity to determine levels of *tara-lacZ* expression in $Bap55^{LL05955}$/+ and wild-type (w^{1118}) regenerating wing pouches at R48. $n = 8$ wing discs ($Bap55^{LL05955}$/+) and nine wing discs (w^{1118}). Error bars are SEM. (H–J) Adult wings after disc regeneration in wild-type (w^{1118}) (H), osa^{308}/+ (I) and *UAS-tara*/+; osa^{308}/+ (J) animals. Arrows show five anterior-specific markers in the posterior compartment: anterior crossveins (red), alula-like costa bristles (orange), margin vein (green), socketed bristles (blue), and change of wing shape with wider distal portion of the wing, similar to the anterior compartment (purple). Anterior is up for all adult wing images. (K) Quantification of the number of Posterior-to-Anterior transformation markers described above in each wing after damage and regeneration of the disc, comparing *UAS-tara*/+; osa^{308}/+ wings to osa^{308}/+ and wild-type (w^{1118}) wings, $n = 21$ wings (*UAS-tara*/+; osa^{308}/+), $n = 16$ wings (osa^{308}/+) and $n = 34$ wings (w^{1118}), from three independent experiments. ***$P < 0.001$, Chi-square test. Chi-square test measuring *UAS-tara*/+; osa^{308}/+ against w^{1118}, $P = 0.86$, is not significant. Scale bars are 100 μm for all wing discs images. Scale bars are 500 μm for all adult wings images. *$P < 0.05$, **$P < 0.01$, Student's *t*-test for (C) and (G).

The enhanced growth in BAP mutants is caused by ectopic AP boundaries

The increased wing size after disc regeneration in *tara*/+ animals was due to loss of *en* in patches of cells, which generated aberrant juxtaposition of anterior and posterior tissue within the posterior compartment. These ectopic AP boundaries established ectopic Decapentaplegic (Dpp) morphogen gradients (Schuster and Smith-Bolton 2015), which can stimulate extra growth in the posterior compartment (Tanimoto *et al.* 2000). To determine whether the *osa*/+ regenerating discs also had ectopic AP boundaries and ectopic morphogen gradients, we immunostained for Ptc to mark AP boundaries and phospho-Smad (pSmad) to visualize gradients of Dpp signaling. Indeed, ectopic regions of Ptc expression were surrounded by ectopic pSmad gradients in osa^{308}/+ regenerating

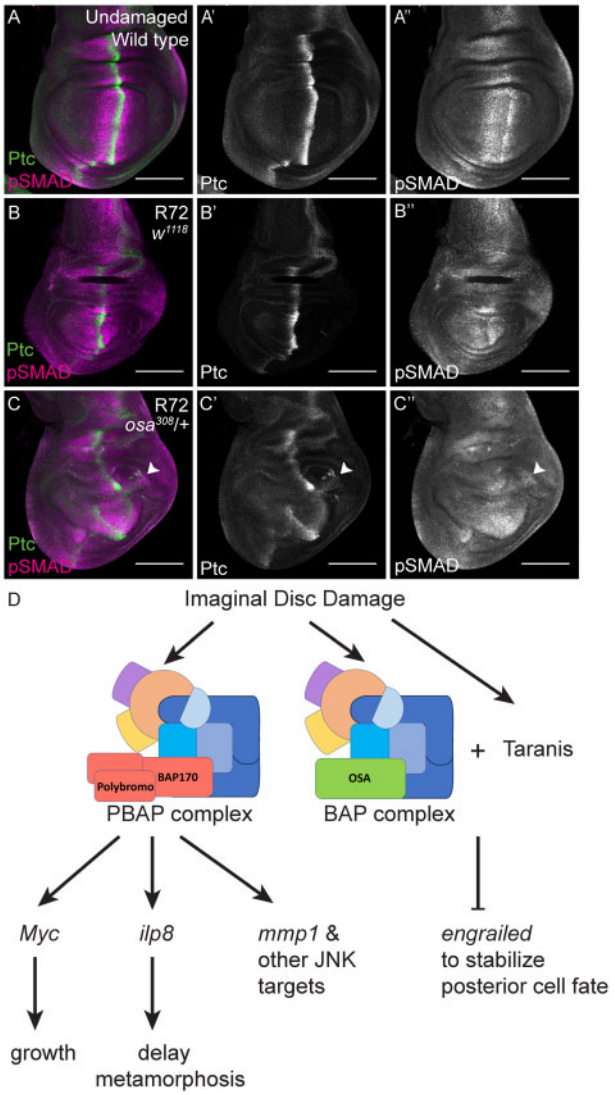

Figure 8 Cell fate changes induce ectopic AP boundaries in the posterior compartment during wing disc regeneration. (A) Wild-type (w^{1118}) undamaged wing disc with Ptc (green) (A′) and pSMAD (magenta) (A″) immunostaining. (B) Wild-type (w^{1118}) regenerating wing disc at R48 with Ptc (green) (B′) and pSMAD (magenta) (B″) immunostaining. (C) osa^{308}/+ regenerating wing disc at R48 with Ptc (green) (C′) and Ci (magenta) (C″) immunostaining. (D) Proposed working model for the functions of the PBAP and BAP complexes in regeneration.

discs (Figure 8, A–C). Thus, the enhanced regeneration in osa^{308}/+ and other SWI/SNF mutant animals was likely a secondary result of the patterning defect. Furthermore, pupariation occurred later in osa^{308}/+ regenerating animals compared to w^{1118} regenerating animals (Supplementary Figure S6, G and H), which provided more time for regeneration in the mutants. Such a delay in pupariation can be caused by aberrant proliferation (Colombani *et al.* 2012; Garelli *et al.* 2012) in addition to tissue damage, and the combination of the two likely led to the increase in delay in metamorphosis seen specifically in mutants with P-to-A transformations.

Discussion

To address the question of how regeneration genes are regulated in response to tissue damage, we screened a collection of mutants and RNAi lines that affect a significant number of the chromatin regulators in *Drosophila*. Most of these mutants had regeneration phenotypes, confirming that these genes are important for both promoting and constraining regeneration and likely facilitate the shift from the normal developmental program to the regeneration program, and back again. The variation in regeneration phenotypes among different chromatin regulators and among components of the same multiunit complexes supports our previous finding that damage activates expression of genes that both promote and constrain regeneration (Khan *et al.* 2017). Such regulators of regeneration may be differentially affected by distinct mutations that affect the same chromatin-modifying complexes, resulting in different phenotypes.

We have demonstrated that both *Drosophila* SWI/SNF complexes play essential but distinct roles during epithelial regeneration, controlling multiple aspects of the process, including growth, developmental timing, and cell fate (Figure 8D). Furthermore, our work has identified multiple likely targets, including *mmp1*, *Myc*, *ilp8*, and *en*. Indeed, analysis of data from a recent study that identified regions of the genome that transition to open chromatin after imaginal disc damage showed such damage-responsive regions near *Myc*, *mmp1*, and *ilp8* (Vizcaya-Molina *et al.* 2018). While previous work has suggested that chromatin modifiers can regulate regeneration (Wang *et al.* 2008; Stewart *et al.* 2009; Blanco *et al.* 2010; Scimone *et al.* 2010; Tseng *et al.* 2011; Fukuda *et al.* 2012; Jin *et al.* 2013, 2015; Xiong *et al.* 2013; Pfefferli *et al.* 2014; Skinner *et al.* 2015; Sun *et al.* 2016), and that the chromatin near *Drosophila* regeneration genes is modified after damage (Harris *et al.* 2016; Vizcaya-Molina *et al.* 2018), our results suggest that these damage-responsive loci are not all coordinately regulated in the same manner. The SWI/SNF complexes target different subsets of genes, and it will not be surprising if different cofactors or transcription factors recruit different complexes to other subsets of regeneration genes.

Is the requirement for the SWI/SNF complexes for growth and conservation of cell fate in the wing disc specific to regeneration? In contrast to *tara*, which is required for posterior wing fate only after damage and regeneration (Schuster and Smith-Bolton 2015), loss of *mor* in homozygous clones during wing disc development caused loss of *en* expression in the posterior compartment (Brizuela and Kennison 1997), although this result was interpreted to mean that *mor* promotes rather than constrains *en* expression, which is the opposite of our observations. Importantly, undamaged *mor* heterozygous mutant animals did not show patterning defects (Supplementary Figure S2, E and F), while damaged heterozygous mutant animals did (Figure 3E), indicating that regenerating tissue is more sensitive to reductions in SWI/SNF levels than normally developing tissue. Furthermore, *osa* is required for normal wing growth (Terriente-Félix and de Celis 2009), but reduction of *osa* levels did not compromise growth during regeneration (Supplementary Figure S3, D–H), and instead led to enhanced regeneration (Figure 2D). Thus, while some functions of SWI/SNF during regeneration may be the same as during development, other functions of SWI/SNF may be unique to regeneration.

SWI/SNF complexes help organisms respond rapidly to stressful conditions or changes in the environment. For example, SWI/SNF is recruited by the transcription factor DAF-16/FOXO to promote stress resistance in *Caenorhabditis elegans* (Riedel *et al.* 2013), and the *Drosophila* BAP complex is required for the activation of target genes of the NF-κB signaling transcription factor Relish in immune responses (Bonnay *et al.* 2014). Here we show that the *Drosophila* PBAP complex is similarly required after tissue damage for activation of target genes of the JNK signaling transcription

factor AP-1 after tissue damage. Interestingly, the BAF60a subunit, a mammalian homolog of *Drosophila* BAP60, directly binds the AP-1 transcription factor and stimulates the DNA-binding activity of AP-1 (Ito *et al.* 2001), suggesting that this role may be conserved.

In summary, we have demonstrated that the two SWI/SNF complexes regulate different aspects of wing imaginal disc regeneration, implying that activation of the regeneration program is controlled by changes in chromatin, but that the mechanism of regulation is likely different for subsets of regeneration genes. Future identification of all genes targeted by BAP and PBAP after tissue damage, the factors that recruit these chromatin-remodeling complexes, and the changes they induce at these loci will deepen our understanding of how unexpected or stressful conditions lead to rapid activation of the appropriate genes.

Acknowledgments

The authors would like to thank A. Brock and K. Schuster for critical reading of the manuscript and helpful discussions; A. Dingwall, D. Bohmann, J. Kennison, J. Treisman, M Cleary, S. Cohen, the Bloomington Drosophila Stock Center (NIH P40OD018537), the Vienna *Drosophila* Resource Center, and the Developmental Studies Hybridoma Bank for fly stocks and reagents.

Funding

This work was supported by a Young Investigator Award from the Roy J. Carver Charitable Trust (#12-4041) (https://www.carvertrust.org) and a grant from the National Institutes of Health (NIGMS R01GM107140) (https://www.nigms.nih.gov).

Conflicts of interest

None declared.

Literature cited

Becker PB, Workman JL. 2013. Nucleosome remodeling and epigenetics. Cold Spring Harb Perspect Biol. 5:a017905.

Bergantinos C, Corominas M, Serras F. 2010. Cell death-induced regeneration in wing imaginal discs requires JNK signalling. Development. 137:1169–1179.

Blanco E, Ruiz-Romero M, Beltran S, Bosch M, Punset A, *et al.* 2010. Gene expression following induction of regeneration in Drosophila wing imaginal discs. Expression profile of regenerating wing discs. BMC Dev Biol. 10:94.

Bonnay F, Nguyen X-H, Cohen-Berros E, Troxler L, Batsche E, *et al.* 2014. Akirin specifies NF-B selectivity of Drosophila innate immune response via chromatin remodeling. EMBO J. 33:2349–2362.

Bosch M, Bagun J, Serras F. 2008. Origin and proliferation of blastema cells during regeneration of *Drosophila* wing imaginal discs. Int J Dev Biol. 52:1043–1050.

Brizuela BJ, Kennison JA. 1997. The *Drosophila* homeotic gene *moira* regulates expression of *engrailed* and HOM genes in imaginal tissues. Mech Dev. 65:209–220.

Brock AR, Seto M, Smith-Bolton RK. 2017. Cap-n-collar promotes tissue regeneration by regulating ROS and JNK signaling in the *Drosophila* wing imaginal disc. Genetics. 206:1505–1520.

Capdevila J, Estrada MP, Sánchez-Herrero E, Guerrero I. 1994. The *Drosophila* segment polarity gene *patched* interacts with *decapentaplegic* in wing development. EMBO J. 13:71–82.

Carrera I, Zavadil J, Treisman JE. 2008. Two subunits specific to the PBAP chromatin remodeling complex have distinct and redundant functions during *Drosophila* development. Mol Cell Biol. 28:5238–5250.

Chalkley G E, Moshkin Y M, Langenberg K, Bezstarosti K, Blastyak A, *et al.*. 2008. The Transcriptional Coactivator SAYP Is a Trithorax Group Signature Subunit of the PBAP Chromatin Remodeling Complex. MCB. **28**:2920–2929. 10.1128/MCB.02217-07

Chatterjee N, Bohmann D. 2012. A versatile ΦC31 based reporter system for measuring AP-1 and Nrf2 signaling in *Drosophila* and in tissue culture. PLoS One. 7:e34063.

Collins RT, Furukawa T, Tanese N, Treisman JE. 1999. Osa associates with the Brahma chromatin remodeling complex and promotes the activation of some target genes. EMBO J. 18:7029–7040.

Collins RT, Treisman JE. 2000. Osa-containing Brahma chromatin remodeling complexes are required for the repression of wingless target genes. Genes Dev. 14:3140–3152.

Colombani J, Andersen DS, Léopold P. 2012. Secreted peptide Dilp8 coordinates *Drosophila* tissue growth with developmental timing. Science. 336:582–585.

Cook RK, Christensen SJ, Deal JA, Coburn RA, Deal ME, *et al.* 2012. The generation of chromosomal deletions to provide extensive coverage and subdivision of the *Drosophila melanogaster* genome. Genome Biol. 13:R21.

Côté J, Quinn J, Workman JL, Peterson CL. 1994. Stimulation of GAL4 derivative binding to nucleosomal DNA by the yeast SWI/SNF complex. Science. 265:53–60.

Eaton S, Kornberg TB. 1990. Repression of *ci-D* in posterior compartments of *Drosophila* by *engrailed*. Genes Dev. 4:1068–1077.

Elfring LK, Daniel C, Papoulas O, Deuring R, Sarte M, *et al.* 1998. Genetic analysis of *brahma*: the Drosophila homolog of the yeast chromatin remodeling factor SWI2/SNF2. Genetics. 148:251–265.

Fukuda A, Morris JP, Hebrok M. 2012. Bmi1 is required for regeneration of the exocrine pancreas in mice. Gastroenterology. 143:821–831.e2.

Garelli A, Gontijo AM, Miguela V, Caparros E, Dominguez M. 2012. Imaginal discs secrete insulin-like peptide 8 to mediate plasticity of growth and maturation. Science. 336:579–582.

Grusche FA, Degoutin JL, Richardson HE, Harvey KF. 2011. The Salvador/Warts/Hippo pathway controls regenerative tissue growth in *Drosophila melanogaster*. Dev Biol. 350:255–266.

Gutierrez L. 2003. The *Drosophila* trithorax group gene *tonalli*(*tna*) interacts genetically with the Brahma remodeling complex and encodes an SP-RING finger protein. Development. 130:343–354.

Hargreaves DC, Crabtree GR. 2011. ATP-dependent chromatin remodeling: genetics, genomics and mechanisms. Cell Res. 21:396–420.

Hariharan IK, Serras F. 2017. Imaginal disc regeneration takes flight. Curr Opin Cell Biol. 48:10–16.

Harris RE, Setiawan L, Saul J, Hariharan IK. 2016. Localized epigenetic silencing of a damage-activated WNT enhancer limits regeneration in mature *Drosophila* imaginal discs. Elife. 5:e11588.

Hopmann R, Duncan D, Duncan I. 1995. Transvection in the *Iab-5,6,7* region of the bithorax complex of Drosophila: homology independent interactions in trans. Genetics. 139:815–833.

Ito T, Yamauchi M, Nishina M, Yamamichi N, Mizutani T, *et al.* 2001. Identification of SWI·SNF complex subunit BAF60a as a determinant of the transactivation potential of Fos/Jun Dimers. J Biol Chem. 276:2852–2857.

Jin J, Hong I-H, Lewis K, Iakova P, Breaux M, *et al.* 2015. Cooperation of C/EBP family proteins and chromatin remodeling proteins is essential for termination of liver regeneration. Hepatology. 61:315–325.

Jin Y, Xu J, Yin M-X, Lu Y, Hu L, *et al.* 2013. Brahma is essential for Drosophila intestinal stem cell proliferation and regulated by Hippo signaling. Elife. 2:e00999.

Kassis JA, Kennison JA, Tamkun JW. 2017. Polycomb and trithorax group genes in *Drosophila*. Genetics. 206:1699–1725.

Katsuyama T, Comoglio F, Seimiya M, Cabuy E, Paro R. 2015. During *Drosophila* disc regeneration, JAK/STAT coordinates cell proliferation with Dilp8-mediated developmental delay. Proc Natl Acad Sci USA. 112:E2327–E2336.

Kennison JA, Tamkun JW. 1988. Dosage-dependent modifiers of polycomb and antennapedia mutations in *Drosophila*. Proc Natl Acad Sci USA. 85:8136–8140.

Khan SJ, Abidi SNF, Skinner A, Tian Y, Smith-Bolton RK. 2017. The Duox maturation factor is a key component of a positive feedback loop that sustains regeneration signaling. PLoS Genet. 13: e1006937.

Kornberg T, Sidén I, O'Farrell P, Simon M. 1985. The *engrailed* locus of drosophila: In situ localization of transcripts reveals compartment-specific expression. Cell. 40:45–53.

Kwon H, Imbalzano AN, Khavari PA, Kingston RE, Green MR. 1994. Nucleosome disruption and enhancement of activator binding by a human SW1/SNF complex. Nature. 370:477–481.

Manansala MC, Min S, Cleary MD. 2013. The Drosophila SERTAD protein Taranis determines lineage-specific neural progenitor proliferation patterns. Dev Biol. 376:150–162.

Mashtalir N, D'Avino AR, Michel BC, Luo J, Pan J, *et al.* 2018. Modular organization and assembly of SWI/SNF family chromatin remodeling complexes. Cell. 175:1272–1288.

Mohrmann L, Langenberg K, Krijgsveld J, Kal AJ, Heck AJR, *et al.* 2004. Differential targeting of two distinct SWI/SNF-related *Drosophila* chromatin-remodeling complexes. Mol Cell Biol. 24:3077–3088.

Moshkin YM, Mohrmann L, van Ijcken WFJ, Verrijzer CP. 2007. Functional differentiation of SWI/SNF remodelers in transcription and cell cycle control. Mol Cell Biol. 27:651–661.

Motzny CK, Holmgren R. 1995. The *Drosophila* cubitus interruptus protein and its role in the *wingless* and *hedgehog* signal transduction pathways. Mech Dev. 52:137–150.

Nagl NG, Zweitzig DR, Thimmapaya B, Beck GR, Moran E. 2006. The *c-myc* gene is a direct target of mammalian SWI/SNF–related complexes during differentiation-associated cell cycle arrest. Cancer Res. 66:1289–1293.

Ng M, Diaz-Benjumea FJ, Vincent J-P, Wu J, Cohen SM. 1996. Specification of the wing by localized expression of wingless protein. Nature. 381:316–318.

Page-McCaw A, Serano J, Santé JM, Rubin GM. 2003. *Drosophila* matrix metalloproteinases are required for tissue remodeling, but not embryonic development. Dev Cell. 4:95–106.

Patel NH, Martin-Blanco E, Coleman KG, Poole SJ, Ellis MC, *et al.* 1989. Expression of engrailed proteins in arthropods, annelids, and chordates. Cell. 58:955–968.

Perkins KK, Dailey GM, Tjian R. 1988. Novel Jun-and Fos-related proteins in *Drosophila* are functionally homologous to enhancer factor AP-1. EMBO J. 7:4265–4273.

Pfefferli C, Müller F, Jaźwińska A, Wicky C. 2014. Specific NuRD components are required for fin regeneration in zebrafish. BMC Biol. 12:30.

Phillips RG, Roberts IJ, Ingham PW, Whittle JR. 1990. The *Drosophila* segment polarity gene *patched* is involved in a position-signalling mechanism in imaginal discs. Development. 110:105–114.

Riedel CG, Dowen RH, Lourenco GF, Kirienko NV, Heimbucher T, *et al.* 2013. DAF-16 employs the chromatin remodeller SWI/SNF to promote stress resistance and longevity. Nat Cell Biol. 15:491–501.

Santabárbara-Ruiz P, López-Santillán M, Martínez-Rodríguez I, Binagui-Casas A, Pérez L, *et al.* 2015. ROS-induced JNK and p38 signaling is required for unpaired cytokine activation during *Drosophila* regeneration. PLoS Genet. 11:e1005595.

Schubiger M, Sustar A, Schubiger G. 2010. Regeneration and transdetermination: the role of wingless and its regulation. Dev Biol. 347: 315–324.

Schuldiner O, Berdnik D, Levy JM, Wu JS, Luginbuhl D, *et al.* 2008. piggyBac-based mosaic screen identifies a postmitotic function for cohesin in regulating developmental axon pruning. Dev Cell. 14:227–238.

Schuster KJ, Smith-Bolton RK. 2015. Taranis protects regenerating tissue from fate changes induced by the wound response in *Drosophila*. Dev Cell. 34:119–128.

Scimone ML, Meisel J, Reddien PW. 2010. The Mi-2-like Smed-CHD4 gene is required for stem cell differentiation in the planarian *Schmidtea mediterranea*. Development. 137:1231–1241.

Skeath JB, Carroll SB. 1991. Regulation of *achaete-scute* gene expression and sensory organ pattern formation in the *Drosophila* wing. Genes Dev. 5:984–995.

Skeath JB, Carroll SB. 1992. Regulation of proneural gene expression and cell fate during neuroblast segregation in the *Drosophila* embryo. Dev Camb Engl. 114:939–946.

Skinner A, Khan SJ, Smith-Bolton RK. 2015. Trithorax regulates systemic signaling during *Drosophila* imaginal disc regeneration. Development. 142:3500–3511.

Smith-Bolton RK, Worley MI, Kanda H, Hariharan IK. 2009. Regenerative growth in *Drosophila* imaginal discs is regulated by Wingless and Myc. Dev Cell. 16:797–809.

Spradling AC, Stern DM, Kiss I, Roote J, Laverty T, *et al.* 1995. Gene disruptions using P transposable elements: an integral component of the *Drosophila* genome project. Proc Natl Acad Sci USA. 92: 10824–10830.

Stewart S, Tsun Z-Y, Belmonte JCI. 2009. A histone demethylase is necessary for regeneration in zebrafish. Proc Natl Acad Sci USA. 106:19889–19894.

Sun G, Irvine KD. 2011. Regulation of Hippo signaling by Jun kinase signaling during compensatory cell proliferation and regeneration, and in neoplastic tumors. Dev Biol. 350:139–151.

Sun X, Chuang J-C, Kanchwala M, Wu L, Celen C, *et al.* 2016. Suppression of the SWI/SNF component *Arid1a* promotes mammalian regeneration. Cell Stem Cell. 18:456–466.

Tamkun JW, Deuring R, Scott MP, Kissinger M, Pattatucci AM, *et al.* 1992. brahma: a regulator of Drosophila homeotic genes structurally related to the yeast transcriptional activator SNF2SWI2. Cell. 68:561–572.

Tanimoto H, Itoh S, ten Dijke P, Tabata T. 2000. Hedgehog creates a gradient of DPP activity in *Drosophila* wing imaginal discs. Mol Cell. 5:59–71.

Terriente-Félix A, de Celis JF. 2009. Osa, a subunit of the BAP chromatin-remodelling complex, participates in the regulation of gene expression in response to EGFR signalling in the *Drosophila* wing. Dev Biol. 329:350–361.

Treisman JE, Luk A, Rubin GM, Heberlein U. 1997. *eyelid* antagonizes *wingless* signaling during *Drosophila* development and has homology to the Bright family of DNA-binding proteins. Genes Dev. 11: 1949–1962.

Tseng A-S, Carneiro K, Lemire JM, Levin M. 2011. HDAC activity is required during *Xenopus* tail regeneration. PLoS One. 6: e26382.

Vázquez M, Moore L, Kennison JA. 1999. The trithorax group gene *osa* encodes an ARID-domain protein that genetically interacts with the brahma chromatin-remodeling factor to regulate transcription. Development. 126:733–742.

Vizcaya-Molina E, Klein CC, Serras F, Mishra RK, Guigó R, *et al.* 2018. Damage-responsive elements in *Drosophila* regeneration. Genome Res. 28:1852–1866.

Wang G-L, Salisbury E, Shi X, Timchenko L, Medrano EE, *et al.* 2008. HDAC1 cooperates with C/EBPalpha in the inhibition of liver proliferation in old mice. J Biol Chem. 283:26169–26178.

Wilson BG, Roberts CWM. 2011. SWI/SNF nucleosome remodellers and cancer. Nat Rev Cancer. 11:481–492.

Xiao H, Sandaltzopoulos R, Wang HM, Hamiche A, Ranallo R, *et al.* 2001. Dual functions of largest NURF subunit NURF301 in nucleosome sliding and transcription factor interactions. Mol Cell. 8: 531–543.

Xiong Y, Li W, Shang C, Chen RM, Han P, *et al.* 2013. Brg1 governs a positive feedback circuit in the hair follicle for tissue regeneration and repair. Dev Cell. 25:169–181.

Zraly CB, Marenda DR, Nanchal R, Cavalli G, Muchardt C, *et al.* 2003. SNR1 is an essential subunit in a subset of *Drosophila* brm complexes, targeting specific functions during development. Dev Biol. 253:291–308.

Communicating editor: R. Duronio